PREPARATION AND CHARACTERIZATION OF HYDROGEN-BONDED
LAYER-BY-LAYER POLYMER FILMS CONTAINING MAGNETIC
NANOPARTICLES

A THESIS SUBMITTED TO
THE GRADUATE SCHOOL OF NATURAL AND APPLIED SCIENCES
OF
MIDDLE EAST TECHNICAL UNIVERSITY

BY

MUHAMMAD ALYAAN AHMED KHAN

IN PARTIAL FULFILLMENT OF THE REQUIREMENTS
FOR THE DEGREE OF MASTER OF SCIENCE
IN
POLYMER SCIENCE AND TECHNOLOGY

AUGUST 2014

Approval of the thesis:

PREPARATION AND CHARACTERIZATION OF HYDROGEN-BONDED LAYER-BY-LAYER POLYMER FILMS CONTAINING MAGNETIC NANOPARTICLES

Submitted by **MUHAMMAD ALYAAN AHMED KHAN** in partial fulfillment of the requirements for the degree of **Master of Science in Polymer Science and Technology Department, Middle East Technical University** by,

Prof. Dr. Canan Özgen   _____
Dean, Graduate School of **Natural and Applied Sciences**

Prof. Dr. Teomen Tinçer   _____
Head of Department, **Polymer Science and Technology**

Assist. Prof. Dr. İrem Erel Göktepe   _____
Supervisor, **Polymer Science and Technology Dept., METU**

Examining Committee Members:

Prof.Dr.Jale Hacaloğlu   _____
Polymer Science and Technology Dept., METU

Assist. Prof. Dr. İrem Erel Göktepe   _____
Polymer Science and Technology Dept., METU

Assoc. Prof. Dr. Ali Çırpan   _____
Polymer Science and Technology Dept., METU

Prof.Dr. Cevdet Kaynak   _____
Polymer Science and Technology Dept., METU

Assoc. Prof. Dr. Gülay Ertaş   _____
Chemistry Dept., METU

Date: 14.08.2014

I hereby declare that all information in this document has been obtained and presented in accordance with academic rules and ethical conduct. I also declare that, as required by these rules and conduct, I have fully cited and referenced all material and results that are not original to this work.

Name, Last name: MUHAMMAD ALYAAN AHMED KHAN

Signature:

ABSTRACT

PREPARATION AND CHARACTERIZATION OF HYDROGEN-BONDED LAYER-BY-LAYER POLYMER FILMS CONTAINING MAGNETIC NANOPARTICLES

Khan, Muhammad Alyaan Ahmed

M.S. Department of Polymer Science and Technology

Supervisor: Assist. Prof. Dr. İrem Erel Göktepe

August 2014, 77 pages

Stimuli responsive layer-by-layer (LbL) polymer films are promising materials as platforms for controlled release of functional biological molecules such as drugs, proteins, growth hormones, etc. from surfaces. Recently, there has been a growing interest for preparation of LbL polymer platforms containing superparamagnetic iron oxide nanoparticles for dual functionality, i.e. bioimaging and controlled delivery of biological molecules. Moreover, if superparamagnetic iron oxide nanoparticles are embedded into temperature-responsive polymer films, an external trigger mechanism, i.e. magnetothermal trigger can also be used to release functional biological molecules on demand from the surfaces.

The study presented in this thesis presents a strategy to incorporate charged iron oxide nanoparticles into neutral hydrogen-bonded polymer LbL films. First, iron oxide nanoparticles with size smaller than 20 nm were synthesized by co-precipitation technique using ultrasonication during synthesis. Iron oxide nanoparticles were characterized using dynamic light scattering, zeta-potential measurements, Fourier

Transform Infrared Microscopy (FTIR) Spectroscopy, X-ray Diffraction (XRD) and Transmission Electron Microscopy (TEM) imaging. For multilayer assembly, polyvinyl caprolactam (PVCL) and tannic acid (TA) were used as polymer building blocks. PVCL is a hydrogen accepting neutral polymer whereas TA has hydrogen donating hydroxyl groups with a pK_a of ~ 8.5. At moderately acidic conditions, TA carries both protonated and ionized hydroxyl groups, thus can interact with PVCL through hydrogen bonding interactions, whereas it associates with positively charged iron oxide nanoparticles through electrostatic interactions. LbL films were constructed at pH 4 by immersing the substrate into solutions of TA, PVCL, TA and iron oxide nanoparticles. This process is repeated in the same order of solutions until desired number of layers is deposited at the surface. Stability of multilayers against pH was examined in detail. Multilayer growth and pH-stability were followed by UV-Visible Spectroscopy. Morphology of the multilayers were characterized using Atomic Force Microscopy (AFM). Information about magnetic properties of multilayers was obtained using Magnetic force Microscopy (MFM).

Multilayers of TA/PVCL/TA/iron oxide nanoparticles were highly stable at acidic and slightly basic conditions. Moreover, these multilayers were capable of releasing ciprofloxacin, an antibiotic used for treatment of different bacterial infections in the body, at neutral and slightly basic conditions at body temperature. Release of ciprofloxacin from the multilayers was followed using UV-Visible Spectroscopy.

The work in this thesis presents the first example of preparation of temperature responsive hydrogen-bonded multilayers containing magnetic iron oxide nanoparticles. In addition to temperature response, multilayers were capable of releasing ciprofloxacin by a pH trigger. Results obtained in this study form a basis for the development of more advanced responsive multilayer films for theranostic (therapeutic and diagnostic) applications.

ÖZ

MANYETIK NANOPARÇACIKLAR İÇEREN HIDROJEN-BAĞLI KATMAN-KATMAN POLIMER FILMLERIN HAZIRLANMASI VE TANIMLANMASI

Khan, Muhammad Alyaan Ahmed

Yüksek Lisans, Polimer Bilim ve Tecknoloji Bölümü

TezYöneticisi: Y.Doç.Dr. İrem Erel Göktepe

Ağustos 2014, 77 sayfa

Ortam koşullarına duyarlı katman-katman polimer filmler ilaç, protein, büyüme hormonları gibi işlevsel biyolojik moleküllerin kontrollü salımı için ümit verici polimerik platformlardır. Son yıllarda, hem biyogörüntüleme hem de biyolojik moleküllerin kontrollü salımını gerçekleştirebilecek iki işlevselliğe sahip süperparamanyetik nanoparçacıklar içeren katman-katman filmlerin hazırlanması yoğun ilgi çekmektedir. Süperparamanyetik nanoparçacıkların sıcaklığa duyarlı polimer filmlerin içerisine yerleştirilmesi durumunda ise harici tetikleme yöntemlerinden biri olan manyetotermal tetikleme aracılığıyla işlevsel biyolojik moleküllerin istenildiği zaman yüzeyden salınmasını mümkün kılmaktadır.

Bu tez çalışması elektriks yüklü demir oksit nanoparçacıklarının nötr hidrojen bağlı katman-katman polimer filmlerin içerisine yerleştirilmesi için bir yolsunmaktadır. İlk olarak, boyutları 20 nm'den küçük manyetik demir oksit nanoparçacıkları "birlikte çöktürme" tekniği ile ultrasound uygulaması eşliğinde sentezlenmiştir. Demir oksit nanoparçacıkları dinamik ışık saçılımı, zeta-potansiyel ölçümü, Infrared Spektroskopisi (IR), X-ışını kırınım yöntemi (XRD), taramalı elektron mikroskobu (TEM) ile görüntüleme yöntemleri ile tanımlanmıştır. Film üretimi için poli (vinil kaprolaktam)

(PVCL) ve Tanik Asit(TA) yapı-taşları olarak kullanılmıştır. PVCL hidrojen alıcı gruplara sahip nötr bir polimer, TA ise hidrojen verici hidroksil gruplara sahip olup yaklaşık pK_a değeri ~ 8.5'tir. Orta derecede asitliğe sahip ortamlarda, TA hem protonlanmış hem de iyonize hidroksil gruplarına sahiptir. Böylece hidrojen bağları aracılığıyla PVCL ile etkileşmesi, elektrostatik bağlar aracılığıyla da demir oksit nanoparçacıkları ile etkileşmesi mümkündür. Katman-katman filmler pH 4'te substratınsırayla TA, PVCL, TA and demir oksit nanoparçacıklar içeren çözeltilere ardışık olarakdaldırılması suretiyle üretilmiştir. Bu işlemistenilen katman sayısına ulaşana kadar substratın aynı sırayı takip ederek çözeltilerin içerisine daldırılması yoluyla devam eder. Filmlerin pH değişimlerine karşı kararlığı detaylı olarak idelenmiştir. Çok-katmanlı filmlerin üretimi ve pH kararlığı UV-Görünür Bölge Spektroskopisi kullanılarak takip edilmiştir. Filmlerin morfolojisi Atomik Kuvvet Mikroskobu (AFM), manyetik özellikleri ise Manyetik Kuvvet Mikroskobu (MFM) kullanarak tanımlanmıştır.

TA/PVCL/TA/demir oksit nanoparçacıklarından oluşan çok-katmanlı filmler asidik ve bazik koşullarda oldukça kararlı davranış gösterdiler. Ayrıca, çok-katmanlı filmlerin yüzeyinden vücut içerisinde farklı bakteriyel infeksiyonların tedavisinde kullanılan ciprofloxacin isimli antibiyotiğin salımı nötr ve hafif bazik pH değerlerinde vücut sıcaklığında başarıyla gerçekleştirilmiştir. Çok-katmanlı filmlerin yüzeyinden ciprofloxacin salımı UV-Görünür Bölge Spektroskopisi kullanılarak takip edilmiştir.

Bu çalışma bilgimiz dahilinde, manyetik demir oksit nanoparçacıkları içerenhidrojen-bağlı sıcaklığa duyarlıpolimer filmlerin hazırlanmasını ve tanımlanmasını gösteren ilk çalışmadır. Filmler, sıcaklık duyarlıklarının yanısıra pH tetiklemesi ile ciprofloxacin isimli antibiyotiğin salımını mümkün kılmaktadır. Bu çalışmadan elde edilen sonuçlar teranostik (tedavi ve teşhis) uygulamalar için daha gelişmiş duyarlı film sistemlerinin üretimi için temel bilgi birikimini oluşturmaktadır.

Anahtar kelimeler: manyetik demir oksit nanoparçacıkları, katman-katman kendiliğinden yapılanma yöntemi, hidrojen-bağlı çok-katmanlı filmler, biyolojik olarak işlevsel moleküllerin kontrollü salımı

To my family,

ACKNOWLEDGEMENTS

TABLE OF CONTENT

LIST OF FIGURES

LIST OF TABLE

LIST OF ABBREVIATIONS

LbL	Layer-by-layer
HB	Hydrogen-bonded
TA	Tannic Acid
BPEI	Branched poly(ethylenimine)
PVCL	poly(*N*-vinylcaprolactam)
PNIPAM	poly(*N*-isopropylacrylamide)
DI	Deionized water
CIPRO	Ciprofloxacin
PSS	poly(styrene sulfonate)
PDADMAC	poly(diallyldimethylammonium chloride)
PAH	poly(allylamine hydrochloride)
PAA	poly(acrylic acid)
PMAA	poly(methyacrylic acid)
LCST	lower critical solution temperature
PVME	poly(vinyl methyl ether)
SPIONs	super paramagnetic iron oxide nanoparticles

CHAPTER 1

INTRODUCTION

1.1. Polymer Multilayer Films:

1.1.1. Polyelectrolyte complexation in solution

Polyelectrolytes are macromolecules whose repeating units bear ionizable groups so that they acquire charges along the macromolecular chain when dissolved in a polar solvent, which is generally water. Basically, there are 2 types of polyelectrolytes, i.e. strong and weak polyelectrolytes. A strong polyelectrolyte dissociates in solution in a wide pH range, whereas a weak polyelectrolyte has a dissociation constant and ionizes partially in solution depending on the solution pH. Figure 1.1 shows examples of strong and weak polyelectrolytes.
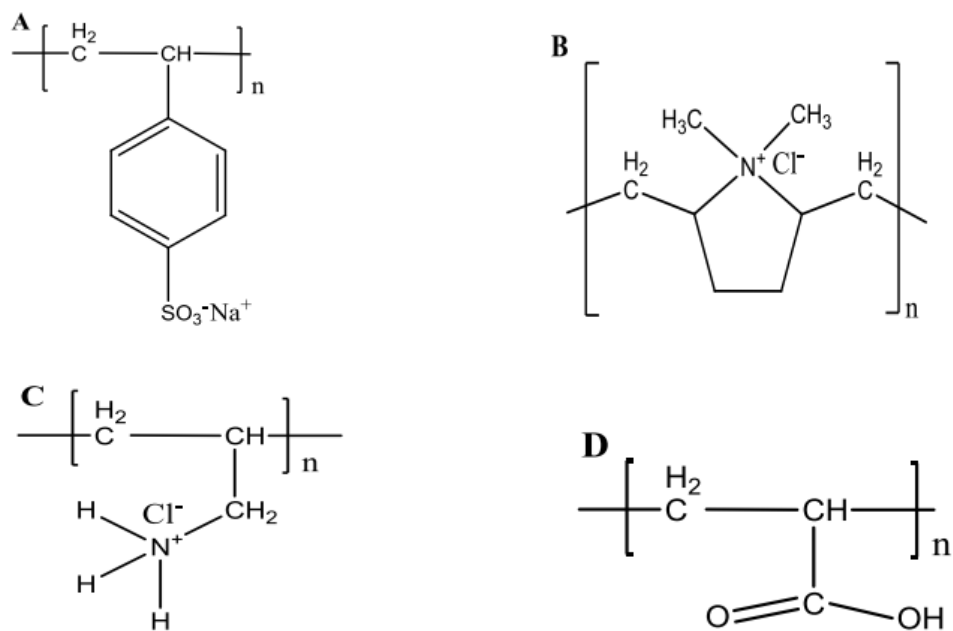
Figure 1.1 Examples of strong polyelectrolyte: (A) Polystyrene sulfonate (PSS) and (B) Polydiallyldimethylammonium chloride (PDADMAC), Examples of weak polyelectrolytes: (C) Polyallylamine hydrochloride (PAH) and (D) Polyacrylic acid (PAA).

Polyelectrolytes behave as both polymers and salts. That's why they are also called "polysalts". The low molar mass counterions are strongly bound to the ionizable groups in the solid state and a polar solvent. Similar to the behaviour of low molar mass salts, the ionizable groups of the polyelectrolytes become solvated in aqueous solution resulting in enhanced mobility of the low molar mass counterions. Polyelectrolyte complexes are formed when solutions of oppositely charged polyelectrolytes are mixed under proper stoichiometry and the oppositely charged polyions associate through electrostatic interactions. Polyelectrolyte complexes exhibit completely different properties than their constituting polyelectrolytes. The major driving force for polyelectrolyte complexation is the gain in entropy caused by the release of low molar

mass salt ions [1]. However, ion-dipole forces and/or hydrophobic interactions also contribute to the complexation process [2]. Figure 1.2 shows schematic representation of polyelectrolyte complexation in solution. As seen in Figure 1.2, polyelectrolyte complexes may consist of both relatively more ordered so called "ladder –like" or disordered co called "scrambled egg" regions [3].
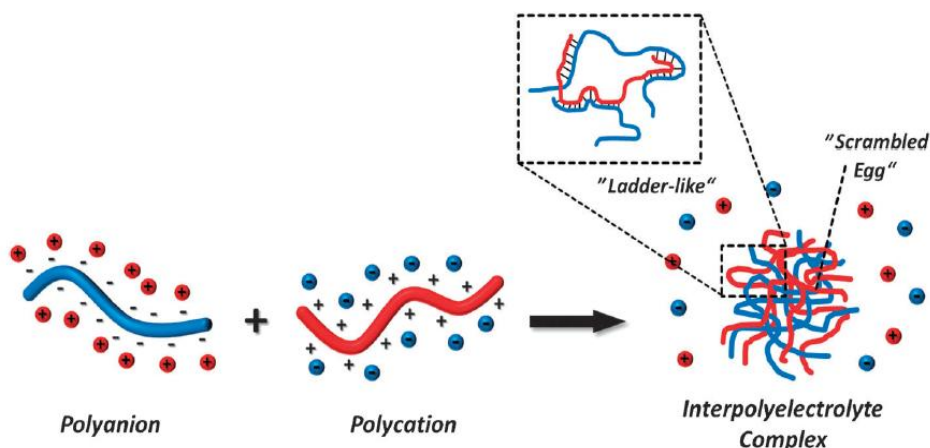
Figure 1.2 Schematic representation of polyelectrolyte complexation and release of low molar mass counterions reprinted with permission from reference [3].

The ratio of the positive to negative charges of the oppositely charged polyelectrolytes is an important parameter in polyelectrolyte complexation. Stoichiometric interpolyelectrolyte complexes are hydrophobic due to mutual screening of the charges and precipitate in solution [3]. However, use of polyelectrolytes with significantly different molecular weights or mixing weak polyelectrolytes with non-stoichiometric ratio result in overcharging due to excess of the either of the polyelectrolytes and formation of water-soluble polyelectrolyte complexes [1,3]. In the latter case, the complex adopts a conformation which is similar to ladder-like structure. Figure 1.3 shows a schematic representation of a water-soluble complex which was suggested by

Kabanov and Zezin [1]. Single-stranded segments show the hydrophilic, whereas double-stranded segments show the hydrophobic parts of the complex.
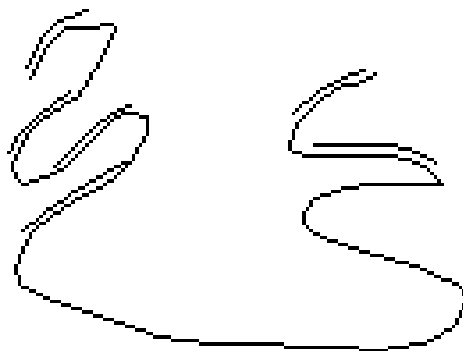
Figure 1.3 Schematic representation of a water-soluble complex based on the schematic presented in reference [1] (Modified from C. Ankerfors, *Licentiate, Royal Institute of Technology,* **2008**).

The structure of the complexes highly depends on the nature of the polyelectrolytes and the external conditions [1,2]. The properties of the polyelectrolyte complexes are specifically affected by the pH, molecular weight of the polyelectrolytes, charge density, concentration of the polyelectrolyte solutions, ionic strength of the solutions and temperature [1]. The first work on interpolyelectrolyte complexation using natural polyelectrolytes with low charge density has been made in the 20th century. Interpolyelectrolyte complexation using synthetic polyelectrolytes was first performed by Fuoss et al in 1949 [6] and followed by Michaels et al. in 1961 [7]. Many other leading studies were reported by Tsuchida [8], Kabanov [9] and Zezin [10] in the following years.

Similar to complexation among polyelectrolytes, polymer complexes can also be obtained through hydrogen bonding interactions among hydrogen accepting and

hydrogen donating polymers. Although the strength of a hydrogen bond is relatively lower than that of an electrostatic bond, the large number of hydrogen bonds which are formed simultaneously among the two hydrogen bonding polymers (cooperative phenomenon) make the interaction strong enough to form hydrogen-bonded interpolymer complexes [4]. Both electrostatic interpolyelectrolyte complexes and hydrogen-bonded interpolymer complexes are of interest due to their wide range of applications. Both types of complexes will be denoted as "interpolymer complexes" in the rest of the thesis.

Interpolymer complexes have recently been of interest in the design of drug delivery systems. The drug molecules can be incorporated into the complexes: i) during complexation, ii) after complexation by absorbing from the solution into the already prepared complexes, iii) by chemically coupling to one of the polymers prior to complexation and iv) the drug molecule itself can participate in complexation. Interpolymer complexes also find use in membrane technology [11], isolation of proteins [12] and nucleic acids [13], fuel cell technology [14], as supports for catalyst [15], preparation of polymer multilayer films at flat [16] and colloidal substrates [17] via layer-by-layer (LbL) technique.

1.1.2. Polyelectrolyte complexation at surfaces: Multilayer Film Assembly

Similar to formation of interpolyelectrolyte complexes by mixing solutions of oppositely charged polymers, polyelectrolyte complexes can also be obtained at the surface by consecutive deposition of oppositely charged polyelectrolytes onto a substrate, so called "layer-by-layer self-assembly technique". This results in construction of polyelectrolyte multilayers at the surface.

In fact, LbL was first introduced by Iler nearly 50 years ago in 1966 [18], by showing alternating deposition of oppositely charged colloidal particles on a glass surface. LbL

was not so popular until it was redeemed by Decher et al. during early 1990`s by using charged polymers for functionalization of surfaces [19]. Rediscovery of LbL by Decher et al. caused a lot of researchers to use LbL technique for functionalization of surfaces which is proved with a huge increase in publications since last two decades [20].

Multilayers of oppositely charged polymers, so called "electrostatic multilayers" using LbL technique is prepared by the following steps: 1) dipping the substrate into a positively charged polyelectrolyte solution; 2) rinsing the substrate with de-ionized water to remove loosely bonded polyelectrolyte chains; 3) immersing the substrate into the counter charge polyelectrolyte solution; 4) rinsing the substrate with de-ionized water to remove the loosely bonded polyelectrolyte chains. The above mentioned process is termed as one bi-layer and it is continued until desired number of layers is achieved. Coating of the polymer on the surface is continued until the charge on the surface is fully compensated. Figure 1.4 shows schematic representation of LbL film preparation process.

1) Polycation Solution   2) Rinsing Solution   3) Polyanion Solution   4) Rinsing Solution
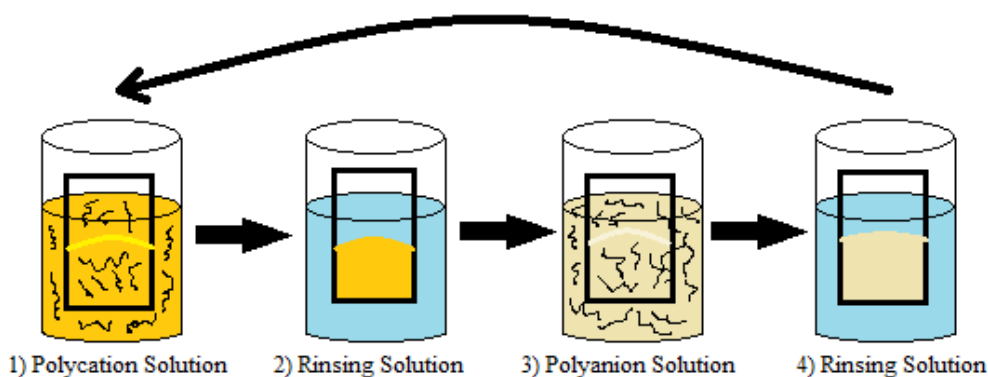
Figure 1.4 Schematic representation of LbL film deposition based on the schematic presented in reference [21] (Modified from Koehler et al., *Chem.Commun.,* **2008).**

As alternatives to dipping process, spray deposition [22, 23] and spin-coating [24] technologies have been developed to speed up the film fabrication process. However, it was found that multilayer film properties are highly affected by the technology used for LbL assembly. For example, spin-coated multilayers are thinner, more transparent and elastic than that produced by dipping technology [47]. Figure 1.5 is obtained from a review by Vincent Ball et al. and summarizes the advantages and disadvantages of the three technologies.
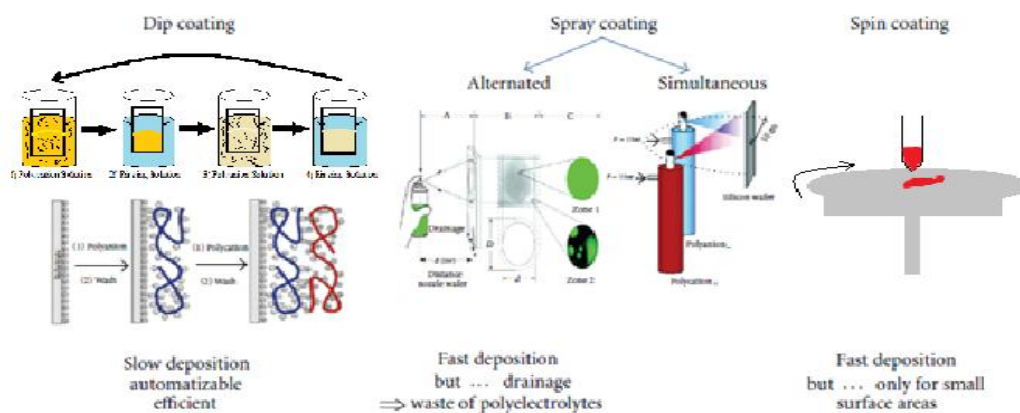
Figure 1.5 Illustration of the dip-, spray-, and spin- coating technologies for fabrication of LbL films presented in reference [47] (Modified from Ball et al. *ISRN Material Science,* **2012**).

LbL self assembly technique offers wide range of advantages over other surface functionalizing techniques for preparation of ultra thin films. The first and the foremost advantage of LbL technique is its simplicity. No expensive or delicate instruments are required for the robust assembly of the layers on the surface [19]. There is no substrate limitation. Glass, quartz, silicon wafer or mica [25] as well as colloidal silica or calcium carbonate nanoparticles can be used as substrates in LbL assembly [26, 27]. LbL films can be prepared in aqueous environment. Therefore, it is an environmentally friendly as

well as a suitable method for biomedical applications [28]. LbL technique does not require any complex chemical reactions as the assembly is accomplished by electrostatic attraction between the polyelectrolytes. Another advantage of LbL technique is that the film properties can be controlled at the assembly and post-assembly steps. Deposition conditions such as pH, ionic strength, polymer concentration, deposition time etc. or post-assembly conditions can all affect the growth as well as ultimate properties of the multilayers [29].

Not only LbL is used to assemble polyelectrolytes but it also provides a wide range of materials to be incorporated within the multilayers. These materials may include inorganic molecular clusters [30, 31], nanoparticles [32, 33], nanotubes and nanowires [34, 35], nanoplates [36, 37], organic dyes [38], dendrimers [39], poryphins [40], nucleic acids and DNA [41], proteins [42-45], and viruses [46]. Providing incorporation of different materials within the multilayers increases the functionality of the surfaces [34].

Similar to interpolyelectrolyte complex formation in solution, multilayer film formation is also not limited to electrostatic interactions among the polymer pairs. Many other interactions such as hydrogen bonding [48-51], electrostatic interactions [52-55], step by step reactions [56-59], sol-gel processes [60-64], molecular recognition and bio recognition [65-68], charge transfer interactions [69-72], electrochemical reactions [73-75] etc. can drive the multilayer film assembly.

Surface functionalizations via LbL assembly technique are in exceeding interest to the researchers because of its potential applications from electronics to biomedical engineering.

1.1.2.1. Stimuli responsive polymer multilayers:

Polymers which are capable of forming non-covalent interactions respond to changes in external stimuli. For example, hydrogen bonding which plays an important role in

determining the secondary structure of biological molecules can be altered by changes in pH, temperature or chemical environment. Thus, polymers capable of forming hydrogen bonding also show response to changes in pH, temperature or chemical environment. In addition to hydrogen bonding polymers, weak polyelectrolytes also show response to pH since the charge density on the polymer can simply be tuned by changing the pH of the solution. In general, small changes in pH and temperature result in an abrupt change in the polymer-polymer and polymer- solvent interactions and conformational changes (transition between extended and compacted coil states) in the polymer. In temperature responsive polymers, small temperature changes around the critical temperature i.e. lower critical solution temperature (LCST) or upper critical solution temperature (UCST) make the chains collapse or to expand responding to the new adjustments of the hydrophobic and hydrophilic interactions between the polymeric chain and the solvent [76]. Similarly, upon ionization of the weak polyelectrolyte, the coiled chains extend dramatically responding to the electrostatic repulsion of the charges (anions or cations) [77]. Non-covalent interactions are not limited to electrostatic or hydrogen bonding interactions. For example, metal-ligand coordination bonding in polymers brings in response to pH and temperature due to reversible breakage and formation of metal-coordination bonds. Stimuli responsive polymers are attracting increasing attention for biomedical applications such as drug delivery, tissue engineering, and bio-sensing [78-82].

Multilayer films which are constructed using responsive polymers or species also show response to changes in environmental stimuli. Stimuli responsive LbL films also pose great application in the fields of nonlinear optics [83], solid state ion conducting materials [84], solar energy conversions [85], and separation membrane [86]. The following subsections will scrutinize the response of LbL films to most common triggers, i.e. pH, ionic strength, temperature and magnetic field.

i.   pH response:

The degree of ionization of the weak polyelectrolytes depends on the pH of their solutions. So the interactions within the multilayers can be easily tuned by just simply changing the pH of the environment. The variation in the pH can result in an increment in the amount of charge and lead to structural changes within the multilayers due to rearrangements of polymeric chains. By taking advantage of these structural changes, properties of the electrostatic multilayers such as permeability, morphology or wettability can be tuned. For example, electrostatic LbL assembly of weak polyelectrolytes, i.e. polyallylamine hydrochloride (PAH) and polyacrylic acid (PAA) when both PAH (pH 7.5) and PAA (pH 3.5) were partially charged resulted in multilayers with loopy layer structure and porous structures were obtained within the multilayers when the multilayers were exposed to strongly acidic conditions followed by a rinse with water at neutral pH. It was also reported that the pH of the solution which the multilayers were exposed to was critical for tuning the size of the pores [87]. For example, exposure to pH 1.8 resulted in pore sizes of 20-40 nm, whereas exposure to pH 2.4 resulted in pore sizes of $\sim$ 1μm. Moreover, sequential exposure to 1.8 and 2.4 resulted in a honey-comb like structure (Figure 1.6).Thus, by simply changing the pH of the medium, internal morphology of the films could be changed which might have significant outcomes in the permeability properties of the multilayers [87].
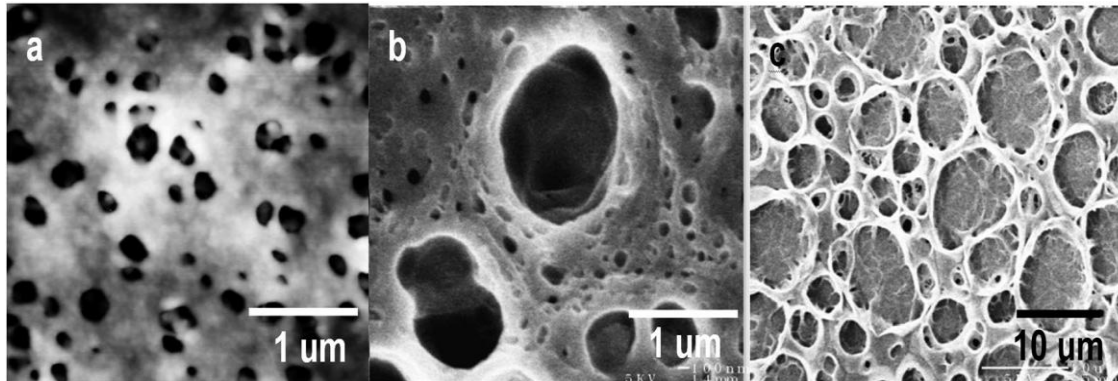
Figure 1.6 Scanning Electron Microscopy images of PAH/PAA multilayers after exposure to pH 1.8 (Panel A); pH 2.4 (Panel B) and sequential exposure to pH 1.8 and 2.4 as presented in reference [87].

Among all types of LbL films, hydrogen bonding-driven multilayers are the most sensitive to pH variations. Sukhishvili and Granick were the first reporting the erasebility of hydrogen-bonded multilayers by a pH trigger. They found that hydrogen-bonded multilayers of a hydrogen accepting neutral polymer, e.g. polyethylene oxide (PEO) and hydrogen donor weak polyacid e.g. polyacrylic acid (PAA) which were constructed at pH 2 when the polyacid was in the protonated form, can be totally erased from the surface by simply increasing the pH to 3.6 [174]. Similarly, hydrogen-bonded multilayers of poly(vinyl pyrrolidone) (PVPON) and polymethyacrylic acid (PMAA) or PEO and PMAA which were prepared at strongly acidic conditions could also be disintegrated when the solution pH was raised to 6.9 and 4.6, respectively [174]. The reason for dissolution of the multilayers was the ionization of the carboxylic acid groups of the polyacids resulting in electrostatic repulsion as well as an increase in osmotic pressure followed by swelling and complete disintegration of the multilayers [88-89]. Response of hydrogen-bonded multilayers at mild pH values makes them promising for controlled delivery of drugs, e.g. wound healing applications.

Complete disintegration of hydrogen bonded multilayers by a simple pH trigger is also advantageous to produce free standing films. For example, by depositing electrostatically bound polyallylamine hydrochloride (PAH) and polystyrene sulfonate (PSS) multilayers onto hydrogen-bonded polyethylene glycol (PEG) and PAA multilayers and exposing the films to pH 5.6-6.3, Decher and co-workers obtained free-standing PAH/PSS multilayers [90]. At pH 5.6-6.3, hydrogen-bonded multilayers of PEG/PAA completely disintegrated, whereas PAH/PSS films remained intact and released into the solution as free-standing films.

ii.   Ionic strength:

The change in ionic strength of the surrounding medium can disrupt electrostatic interactions among the polyelectrolyte pairs due to interactions of the polyelectrolytes with the salt ions. In this ion exchange process, polyelectrolytes do not leave the film but the films remain intact with less number of binding points between the polyelectrolyte layers. Further increasing salt concentration may result in complete disintegration of the multilayers if the remaining polyelectrolyte-polyelectrolyte pairs could no longer keep the multilayers intact. This feature of electrostatic multilayers can be advantageous for controlled release of drug molecules from surfaces.

Weakening the polyelectrolyte-polyelectrolyte interactions by increasing ionic strength of the medium can also result in changes in the permeability of the multilayers. Ibarz et al. showed that LbL capsules produced by using PAH and PSS were impermeable by nature but became permeable to large molecules even when the salt concentration was very low, i.e. 10^{-3} to 10^{-2} M [91]. This was due to a change in polymer conformation (transition from extended to a coiled conformation), providing free path for the molecules to pass through the multilayers. Similarly, nanoporosity can be introduced within the multilayers by increasing ionic strength of the medium. Caruso et al. showed that nanopores could be obtained within the multilayers of polyacrylic acid (PAA) and polyallylamine hydrochloride (PAH) when the films were exposed to salt solutions [92].

These porous membranes could be used as platforms for controlled drug delivery applications.

Response of hydrogen-bonded multilayers to increasing salt concentration of the medium depends on the concentration and type of salt. Kharlampieva and Sukhishvili reported that critical disintegration pH for PVPON/PMAA shifted to lower pH values in the presence of 0.5 M NaCl due to enhanced ionization of the PMAA within the multilayers [93]. Another study reported by Hammond and co-workers showed that multilayers of hydrogen-bonded PEO/PAA could be disintegrated at pH 2.5 only when the concentration of lithium triflate salt was increased to 2 M. High stability of the multilayers can be explained by screening of the negative charges on the partially ionized PAA chains by salt cations resulting in a decrease in the electrostatic repulsion among the PAA chains within the multilayers [94].

iii. Temperature response:

Polymer multilayers can also be made temperature-responsive if at least one of the films components shows temperature-responsive behaviour. Similar to pH-response, temperature-response is mostly observed in hydrogen-bonded multilayers since majority of the temperature responsive polymers are neutral and do not contain ionizable groups for electrostatic self-assembly. The only way to incorporate a neutral polymer into electrostatic multilayers is to introduce monomers with ionizable groups to the neutral polymer through copolymerization.

For example, poly(N-isopropyl acrylamide) (PNIPAM) which is a neutral polymer, has been extensively used in biomedical applications [47] due to its lower critical solution temperature (LCST) of 30-34 °C which is close to body temperature. It has hydrogen accepting carbonyl groups (Figure 1.7), thus can be easily LbL assembled at the surface using a hydrogen donating polymer. There are many examples of hydrogen-bonded multilayers containing PNIPAM [95-97]. In contrast, PNIPAM cannot be used in electrostatic self-assembly unless it is copolymerized with monomers having ionizable groups [98].
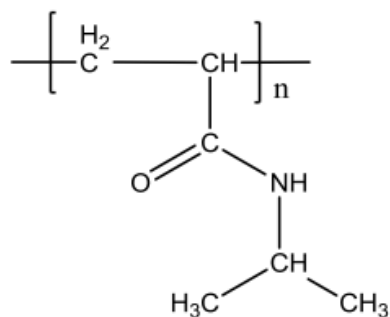
Figure 1.7 Structure of poly(N-isopropyl acrylamide) (PNIPAM).

Temperature response can also trigger the release of drugs from the multilayers. Sukhishvili et al. reported that release of Thymol Blue from hydrogen-bonded

multilayers of poly (methacrylic acid) (PMAA) and temperature responsive poly(N-vinyl caprolactam) (PVCL) or PMAA and temperature responsive poly(vinyl methyl ether) (PVME) increased at temperatures close to the LCSTs of PVCL and PVME, respectively. This was due to phase separation of PVCL or PVME at temperatures close to their LCST, resulting in formation of voids within the multilayers and thereof increased amount of Thymol Blue from the surface [99].

iv.   Magnetic field response:

Magnetic field responsive polymeric multilayers can be produced by incorporating magnetic nanoparticles into the film structure. For example, Lu et al. introduced gold coated ferromagnetic cobalt nanoparticles into LbL capsules prepared from polystyrene sulfonate (PSS) and polyallylamine hydrochloride (PAH) and applied alternating magnetic fields at 100-300 Hz and 1200 Oe strength. They observed permeability of dextran from the multilayers within 30 minutes, indicating the increase in the permeability of LbL capsules. Note that no release of the dextran was observed prior to magnetic field application, proving low or negligible permeability of the capsules [100, 101].

Multilayers containing magnetic nanoparticles are not only of interest for controlled release of functional molecules from the multilayers. Magnetic nanoparticle containing multilayers is also promising for imaging purposes. In addition, exposing magnetic nanoparticle containing multilayers to magnetic field results in localized heating within the film due to hysteresis produced by the nanoparticles. This localized heating effect within the multilayers can trigger release of drug molecules from the surface if the multilayers contain a temperature responsive polymer. Therefore, magnetic nanoparticle containing multilayers are promising for theranostic (therapeutic + diagnostic) applications.

1.2. Preparation of nanometer- scale magnetic nanoparticles:

1.2.1. Introduction to nanoparticles:

Inorganic and/or polymer based nanoparticles have great potential for many different biological and medical applications, e.g. diagnostic test for detection of diseases and drug release applications [102-104].

Super paramagnetic iron oxide nanoparticles (SPIONs) are inorganic nanoparticles, exhibiting magnetic properties which allow directing them to a defined location or heating them in the presence of an externally applied AC magnetic field [105]. For this reason, SPIONs are of interest for many different applications such as separation techniques, magnetic resonance imaging for drug delivery systems, magnetic hyperthermia, and magnetically assisted transfection of cells [106-109].

Among many potential applications of SPIONs, hyperthermia therapy is of growing interest. Magnetic hyperthermia makes use of magnetic nanoparticles as a heat source [110] to raise the temperature to slightly higher values, e.g.to 43 ˚C [111] at the tumor cells. When the SPIONs reach the target tumor site, magnetic hyperthermia is induced with an AC magnetic field which causes the magnetic particles to dissipate heat to the tumor sites [110, 112-115]. The most important factor for a successful treatment is the localization of the SPIONs in order to heat only the tumor cells but not the healthy cells. Until now, different magnetic field strengths, alternating field frequencies and exposure times have been examined for an efficient magnetic hyperthermia therapy [116]. Moreover, different approaches have been developed for localization and/or delivery of SPIONs [116].

1.2.2. Properties of magnetic particles:

1.2.2.1. Magnetic Properties:

The sum of the moments 'm' of the all the atoms per unit volume 'V' is known as magnetization 'M'.

$$M = \frac{m}{V}$$

Susceptibility and permeability describe the response to a magnetic field. Susceptibility 'χ' shows the magnetization level 'M' of a substance under an influence of an external magnetic field 'H' and it is a dimensionless proportionality constant. Permeability, 'μ', is the change in magnetic induction 'B' with the applied magnetic field 'H'.

Permeability can also be described as the measure of conductivity of a material to an applied magnetic field. Therefore, the higher the permeability, the lower will be the resistance of a material to magnetic field. Permeability is measured in Henries per meter (H/m); SI Units. Relative permeability 'μ_r' is calculated as the ratio of materials permeability 'μ' to the permeability of vacuum 'μ_o'.

$$\mu_r = \frac{\mu}{\mu_o}$$

When a material experiences a magnetic field, that material can be classified as the following:

i.   Diamagnetic
ii.   Paramagnetic
iii.   Ferromagnetic
iv.   Super-paramagnetic

i.   Diamagnetic:

When a diamagnetic material is under exposure of a magnetic field, it produces a weak magnetic field in the opposite direction of the applied field. After the removal of the magnetic field, the relaxation of spin occurs and then they settle to their original positions. Diamagnetic has a relative permeability 'μ_r' of less than 1 and susceptibility 'χ' in the range of -10^{-6} to -10^{-3} (it is negative due opposite direction of induced magnetic field) [117].

ii.   Paramagnetic:

When a paramagnetic material is under the exposure of an external magnetic field, it experiences a weak magnetic field in the direction of the field applied. Similar to diamagnetic materials, after the removal of the magnetic field, the attracted spin returns back to normal position and the material becomes demagnetized. Relative permeability 'μ_r'> 1, susceptibility 'χ' $= 10^{-3} – 10^{-5}$. Similar to diamagnetic materials, the response of paramagnetic materials is also weak to an applied magnetic field. Example for the paramagnetic materials is aluminum, oxygen, magnesium, lithium [117].

iii.   Ferromagnetic:

Ferromagnetic materials are the materials with significant amount of magnetic properties. The magnetic moments with or without external magnetic field align in one direction and establish an overall high magnetic moment. The high magnetic moment is observed under a critical temperature known as Curie Temperature. Above Curie Temperature ferromagnetic properties disappear. The material behaves like a paramagnetic material which means that the magnetic moment becomes disordered. Relative permeability is $\mu_r \gg 1$ and susceptibility 'χ' $\gg 1$. Ferromagnetic materials have a multi domain structure. All the moments in one domain are arranged in one direction. The location of the alignment of the moments depends on the crystal structure or crystal defect. Even after the removal of all the external magnetic field, ferromagnetic

materials tend to preserve some amount of magnetization. This feature is known as "remanence magnetization". Examples of ferromagnetic materials are iron, nickel, cobalt and their oxides and alloys of gadolinium, therbium [117].

iv.   Superparamagnetic:

Superparamagnetic materials are specialized form of ferromagnetic materials. When the size of the ferromagnetic material is decreased, this causes a decrease in number of domains. The decreases in the number of domains led the particles turn into a single domain structure [117].

1.2.2.2. Iron Oxides:

Most common materials for the superparamagnetic cores of iron oxide are: magnetite (Fe_3O_4) and maghemite (γ-Fe_2O_3). No magnetic properties were recorded for Wustit (FeO) [118]. Magnetite and maghemite have cubic spinel structures [119].

i.   Magnetite:

Magnetite is formulated with divalent and trivalent Fe ions. IUPAC name of magnetite is iron (II, III) oxide. The chemical formula of magnetite is Fe_3O_4 or $FeO.Fe_2O_3$. Magnetite is found in black or grayish black color mineral. Saturation magnetization of the magnetite at 25 ˚C is 90-92 emu/g [120]. Structural formula $[Fe^{+3}]_{Td} [Fe^{+3,} Fe^{+2}]_{Oh}O^{-2}$ [121], shows tetrahedral magnetic sublattice, which contains Fe^{+3} ions and also an octahedral sublattice which contains Fe^{+3} and Fe^{+2} ions. Spins of the subsequent sublattices are anti-parallel to each other. This means that the net magnetization is due to the Fe^{+2} ions occurring in the octahedral sublattice [122]. Oxidation is a great concern for magnetite because it forms maghemite as soon as it reacts with oxygen.

ii.   Maghemite:

Maghemite is synthesized by the oxidation of magnetite. It contains the trivalent Fe ions. IUPAC name of maghemite is iron (II) oxide and its chemical formula is γ-Fe_2O_3. Maghemite is brown in color. Saturation magnetization of bulk material at 25 ˚C is approximately 80 emu/g. Its crystal structure is almost similar to magnetite but the octahedral regions are occupied by divalent iron ions due to oxidation. Oxidation also causes maghemite to become ferrimagnetic [123].

1.2.2.3. Synthesis of super paramagnetic iron oxide nanoparticles (SPIONs):

A lot of different techniques can be found in literature for the synthesis of SPIONs such as water-in-oil micro-emulsion [124], co-precipitation [125], thermal decomposition of organic iron precursor [126] and others. The SPIONs obtained from these procedures show also different properties such as particle size, shape, size distribution, crystallinity, magnetic properties, etc.

i.   Co-precipitation Method:

One of the easiest as well as earliest methods for synthesis of iron oxide nanoparticles is the co-precipitation of the iron salt such as iron chlorides or sulfates. The first co-precipitation synthesis was performed by Massart et al. more than 30 years ago [127]. The chemistry behind this method is as follows:

$$Fe^{+2} + 2Fe^{+3} + 8OH^- \rightarrow Fe_3O_4 + 4H_2O$$

The above mentioned reaction is consisted of the following steps:

$$(Fe^{+3}(H_2O)_6)^{+3} \rightarrow FeOOH + 3H^+ + 4H_2O$$

$$Fe^{+2} + 2OH^- \rightarrow Fe(OH)_2$$

$$2FeOOH + Fe(OH)_2 \rightarrow Fe_3O_4 + 4H_2O$$
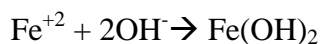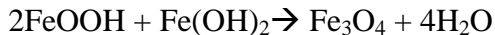
When the iron salts (Fe^{+2} and Fe^{+3} with 1:2 molar ratios) come in contact with an alkaline solution, magnetite is obtained as the precipitate. As discussed before, magnetite is very sensitive to oxidation, thus the process is often carried out under nitrogen or argon gas to prevent the formation of maghemite. This procedure is advantageous as it gives off very high yield [128]. Nanoparticle properties such as size, morphology, magnetic properties are controllable by varying the parameters such as solution pH, ionic strength, temperature, reaction time and nature of the salts.

ii.   Thermal decomposition of iron organic precursor method:

It is possible to obtain mono-dispersed nanoparticles using organometallic precursors through the thermal decomposition method. Organometallic precursors, e.g.hydroxylamineferron [Fe(Cup)$_3$] [129], iron pentacarbonyl [Fe(CO)$_5$] [130], ferric acetylaccetonate [Fe(acac)$_3$] [126], iron oleate [Fe(oleate)$_3$] [131,132] are dissolved in a non-polar solvent and exposed to high temperature. General phenomena in this method are: i) the precursor is heated up to the boiling point of the non-polar solvent under constant heating rate; ii) the mixture is kept at that temperature for desired amount of time. Note that both nucleation and growth are carried out during the heating at the boiling point of the solvent. Thermal decomposition method provides narrow size distribution, high crystallinity and well controlled shape of the nanoparticles [133]. The narrow size distribution is due to the fact that the nucleation and the growth occur at different temperature ranges. Nucleation starts with in the temperature range of 200˚ - 230 ˚C and growth starts within the range of 260˚C - 290˚C.

Size and shape of the particles can be controlled by varying some of the reaction parameters, e.g. temperature of the decomposition reaction, precursor, and duration of the reaction after reaching the boiling point of the solvent. Morphology of the particles can be controlled by the heating rate as well as the precursor: solvent volumetric ratio [134].

The main disadvantage of thermal decomposition method is that the yield per reaction is too low. In addition, organometallic precursors are not environmental friendly, so the researchers look for green synthesis using precursors such as ferric chloride or sodium oleate which are non toxic and environment friendly [135].

1.2.2.4. Incorporation of iron oxide nanoparticles within multilayers:

Size, morphological properties and surface/volume ratio of the magnetic nanoparticles play important role in building up multilayers at surfaces. Size [136] and morphology [137] of the superparamagnetic nanoparticles are advantageous for incorporation into 2D and 3D polymer multilayers assemblies. Magnetic nanoparticles draw attention of polymer chemists to bring also magnetic properties to polymer multilayer films.

LbL technique offers a simple method to incorporate magnetic nanoparticles into multilayers. Using PAH and PSS as the polymer building blocks, Decher et al. successfully incorporated magnetic nanoparticles into electrostatically bound polymer multilayer films and examined the properties of the films with different spatial arrangement of the magnetic nanoparticles [138]. In another study, Liu et al. showed that the iron oxide nanoparticles can be coated with poly (diallyldimethylammonium chloride) (PDDA) and PDDA coated nanoparticles can be LbL assembled at the surface using polyamic acid salt (PAATEA) as the polymer counterpart. It was also reported that coating iron oxide nanoparticles with PDDA increased the monodispersity of the iron oxide nanoparticles by decreasing the coagulation due to electrostatic repulsion among the particles and allowed proper arrangement of nanoparticles within the multilayers [139].

As discussed before in Section 2.2.3. (i), co-precipitation is the most commonly used technique for the synthesis of iron oxide nanoparticles. However, nanoparticles produced by co-precipitation method form aggregates when dissolved in water.

Therefore, iron oxide nanoparticles produced through co-precipitation method are not proper for multilayer assembly due to random distribution of nanoparticles at the surface and difficulty in tuning the magnetic properties [140].

As discussed before in Section 2.2.3. (ii), iron oxide can also be synthesized by thermal decomposition technique. In contrast to co-precipitation technique, thermal decomposition technique provides monodisperse super-paramagnetic nanoparticles via surfactant coating [129]. These monodispersed nanoparticles have good dispersion characteristics, thus are more convenient for multilayer assembly and tuning magnetic properties of the multilayers.

It is worth to note that when the magnetic nanoparticles are incorporated within the polymer multilayers, magnetic properties of nanoparticles are also affected by the dipolar interactions among the nanoparticles. The dipolar interactions among the magnetic nanoparticles are strong enough even to drive the self-assembly of particles onto a surface. For example, the first studies on multilayers of magnetic nanoparticles could be prepared through Langmuir-Blodgett technique [141-144]. Therefore, dipolar interactions among the iron oxide nanoparticles within the polymer multilayers need to be controlled via dimensional arrangement and inter-particle spacing.

Magnetic nanoparticle containing polymer multilayers may find applications in magnetic resonance imaging guided therapy [145] or as adsorbents [146, 147], micromanipulators [147], sensors [148, 149] and microactuators [150, 151].

1.3. Aim of the thesis:

Ultra-thin LbL polymer films are promising materials to functionalize surfaces. If the multilayers show response to environmental conditions, these multilayers can also be used as platforms to release functional molecules from surfaces. Recently, there has been a growing interest to incorporate superparamagnetic iron oxide nanoparticles into

these polymer platforms for bioimaging. In this way, a polymer film can be rendered dually functional, i.e. a surface which can be used for both controlled delivery and bioimaging applications. Polymer coatings containing superparamagnetic iron oxide nanoparticles may also have a potential for controlled delivery of functional molecules through magnetothermal trigger if temperature responsive polymer(s) and superparamagnetic iron oxide nanoparticles reside in the same coating. Application of AC magnetic field will induce heating within the multilayers leading to conformational changes in the temperature responsive polymer which may trigger the release of functional molecules from the surface. Therefore, temperature-responsive multilayers containing superparamagnetic iron oxide nanoparticles can be attractive to prepare theranostic (therapeutic and diagnostic) platforms for treatment of diseases.

As discussed in Section 1.1.2.1, polymers that show response to changes in temperature are mostly neutral polymers with hydrogen accepting groups, e.g. PNIPAM, PVCL, PVME, PEO. These polymers can only be introduced into the multilayers through hydrogen bonding interactions. In contrast, iron oxide nanoparticles are charged species and could be co-assembled at the surface with polymers via electrostatic interactions. For this reason, most of the studies concerning iron oxide nanoparticle containing multilayers are based on electrostatic self-assembly [138, 139]. In this thesis, we aimed to develop a strategy to incorporate iron oxide nanoparticles into hydrogen-bonded multilayers and also examine potential of such multilayers as platforms for controlled release of drug molecules through pH and temperature trigger. Iron oxide nanoparticles with an approximate average diameter of ~ 8 ± 1.5 nm were synthesized through ultrasound based co-precipitation method. For multilayer film assembly, PVCL and TA were used as polymer building blocks. PVCL is a temperature responsive polymer with LCST of 30°C [166] and has hydrogen accepting carbonyl groups. TA, is a natural polyphenol with 25 phenolic hydroxyl groups per molecule and can donate hydrogens to PVCL during multilayer assembly. At the same time, TA can also be rendered partially negatively charged by tuning the solution pH to associate with positively charged iron

oxide nanoparticles. In other words, TA can act as a bridge between PVCL and iron oxide nanoparticles during film assembly. It was found that multilayers of PVCL, TA and iron oxide nanoparticles can be constructed at pH 4 through hydrogen bonding interactions among PVCL and TA and electrostatic interactions among TA and iron oxide nanoparticles. These multilayers were highly stable against pH. Increasing pH to neutral and even basic conditions did not remove materials from the surface. Surface morphology and magnetic properties of iron oxide nanoparticle containing multilayers were examined in detail using AFM and MFM. Finally, potential of the multilayers was examined for controlled release of ciprofloxacin (an antibiotic which is used to treat different types of bacterial infection in the body) at neutral and slightly basic conditions at 37°C. Multilayers were found to release ciprofloxacin at neutral and basic pH at 37-40˚C.

In conclusion, the work presented in this thesis shows the first example of preparation and characterization of iron oxide nanoparticle containing hydrogen-bonded multilayers. To the best of our knowledge, use of MFM was the first attempt to characterize the magnetic properties of polymer multilayers containing iron oxide nanoparticles. Also, loading and pH induced release of ciprofloxacin from hydrogen-bonded polymer multilayers were first demonstrated in this study. These multilayers are promising for both controlled release of functional molecules from surfaces and bioimaging.
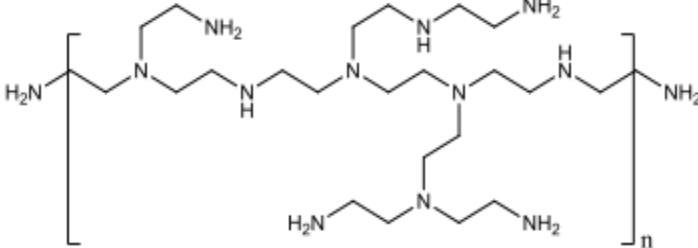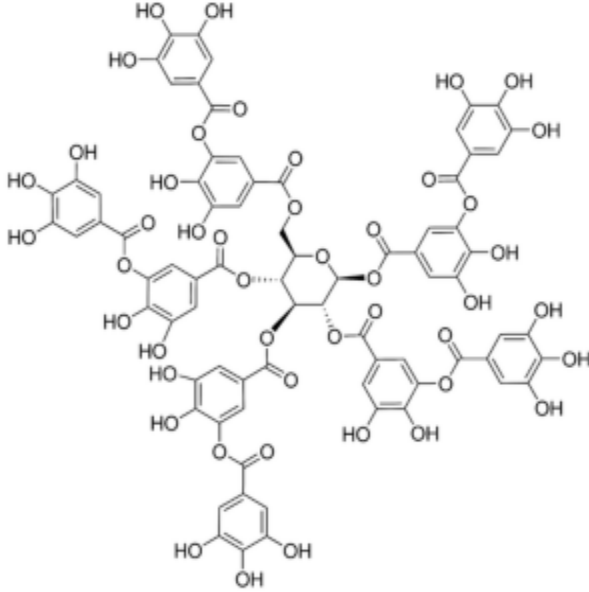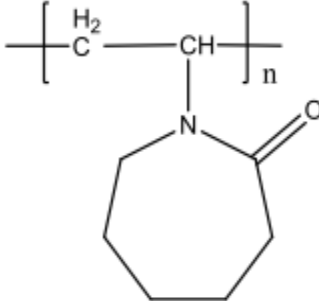
CHAPTER 2

EXPERIMENTAL AND APPARATUS

2.1. Materials:

Iron chloride tetrahydrate ($FeCl_2.4H_2O$) and iron chloride hexahydrate($FeCl_3.6H_2O$) were purchased from Merck Chemicals and Fischer Scientific Company, respectively., Ammonium hydroxide (NH_4OH) (26%) and branched polyethylenimine (BPEI, $M_w = 25,000$) were purchased from Sigma Aldrich. Tannic Acid (TA, $M_w = 1701.20$) was purchased from Merck Chemicals. Polyvinyl caprolactam (PVCL, $M_w = 1800$) was purchased from Polymer Source. Ciprofloxacin was purchased from Fluka Analytical. Table 2.1 shows the structures of the chemicals used and polymers used in this study.

S. No.	Name of the chemical	Structure of the chemical
1	Iron chloride tetrahydrate	
2	Iron chloride hexahydrate	

3	Ammonium Hydroxide	NH_4OH
4	Branched polyethylenimine (BPEI)	
5	Tannic acid (TA)	*http://www.sigmaaldrich.com/catalog/product/sial/403040?lang=en&region=TR
6	Polyvinylcaprolactam (PVCL)	
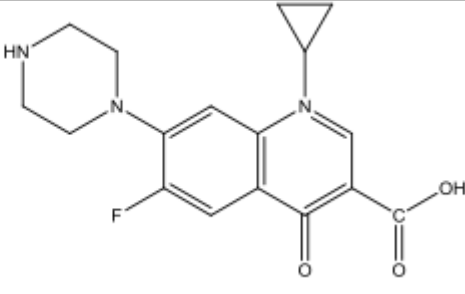
| 7 | Ciprofloxacin (CIPRO) | |

Table 2.1 Structures of the chemicals and polymers.

2.2. Synthesis of Iron Oxide Nanoparticles:

$FeCl_2.4H_2O$ (0.34 g, 1.7 mmol) and $FeCl_3.6H_2O$ (0.95 g, 3.5 mmol) were added into a three-necked round bottom flask which was previously purged with nitrogen gas. Deaerated DI water (20 mL) was added into the three-necked round bottom flask under nitrogen purge and ultrasonication. The mixture was heated for 30 minutes at 50˚C under sonication. After 30 minutes, ammonium hydroxide (2mL) was added dropwise to the reaction mixture. The temperature was kept constant at 50˚C for an additional 30 minutes. Then the resulting mixture was cooled to room temperature. The magnetic particles were collected by a strong magnet. The particles were washed for 6 times with DI water by dispersing the iron oxide nanoparticles in DI water and collecting them using a neodymium strong magnet. The pH of the solution after dispersing iron oxide nanoparticle in DI water was found to be ~ pH 4 [160].

2.3. Multilayer Film Assembly:

Multilayers films were assembled on quartz slides. Quartz slides were cut into 2.5 x 2.5 cm^2 sized squares. The slides were initially treated with concentrated sulfuric acid for 1 hour and 25 minutes to remove the impurities on the surface followed by thorough rinsing with tap water, distilled water and finally with DI water, respectively. Then, the

slides were treated with 0.25 M NaOH solution for 10 minutes. Washing process was repeated as done after acid treatment. The slides were dried by nitrogen gas flow.

PVCL and TA were dissolved in 0.01 M phosphate buffer at pH 4.0. Concentrations of PVCL and TA were 0.2 mg/mL and 0.5 mg/mL, respectively. Prior to multilayer assembly, 1 layer of BPEI was deposited at the surface as a precursor layer for 30 minutes at pH 5. BPEI coated substrates were then immersed into TA, PVCL, TA and iron oxide nanoparticle solutions for 15 minutes in an alternating fashion. Multilayers of TA/PVCL/TA/iron oxide nanoparticles were called as 1-tetralayer throughout the whole thesis. Multilayer growth was followed by measuring the changes in the intensity of the peak centered at 220 nm using UV-Visible Spectroscopy after drying the film coated quartz slides.
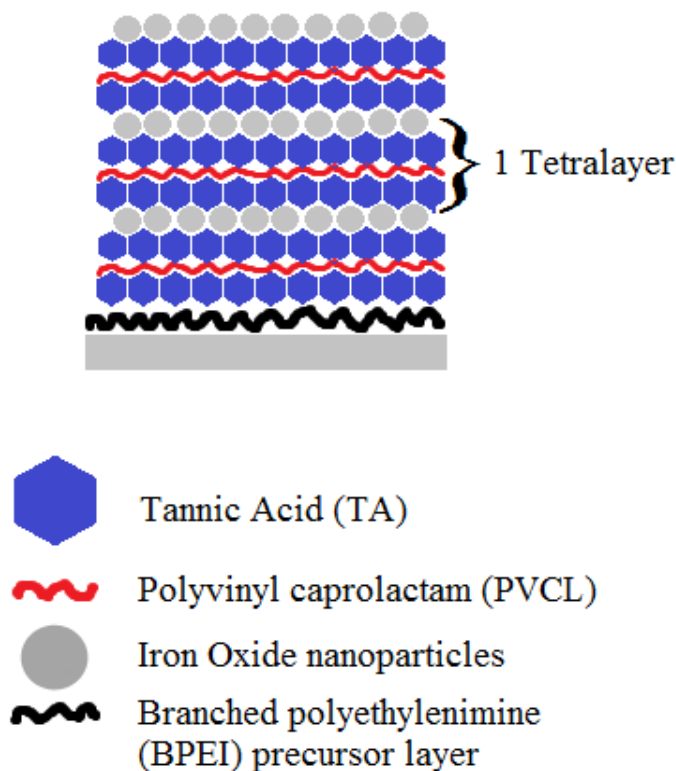
Figure 2.1 Multilayer architecture.

2.4. pH-stability of Multilayers

pH stability of the multilayers were examined by immersing the films into buffer solutions of either decreasing or increasing pH values for 30 minutes. pH-stability of the multilayers were followed by following the evolution of the intensity of the peak centered at 220 nm using UV-Visible Spectroscopy after drying the film coated quartz slides.

2.5. Release of ciprofloxacin from multilayers:

The model drug, ciprofloxacin (CIPRO) was loaded into the multilayers during multilayer assembly. A CIPRO+TA complex was produced by mixing 1.6 mL of 0.25 mg/mL CIPRO solution with 10 mL of 0.5 mg/mL of TA at pH 4.0.Then the multilayers were constructed in a similar fashion as discussed in Section 2.2 (1 tetralayer: TA+CIPRO/PVCL/TA+CIPRO/iron oxide nanoparticles). For ciprofloxacin release experiments, multilayers were coated on both sides of the multilayers (15 tetralayers on each side of the glass slide). Ciprofloxacin release was followed by immersing the multilayer coated glass slides into 0.01 M phosphate buffer solution at pH 7.5 at 37-40 °C. When the release is complete at pH 7.5, release of ciprofloxacin was followed at pH 8.5 at the same temperature.

2.6. Apparatus and Measurement

2.6.1. UV/Vis spectroscopy: Absorption spectra were recorded using a VARIAN Cary 100 Bio-UV/Vis Spectrometer.

2.6.2. Dynamic light scattering (DLS) and zeta-potential measurements: Hydrodynamic sizes and zeta potential measurements of iron oxide nanoparticles were

measured using a ZetasizerNano-ZS equipment (Malvern Instruments Ltd.). Number average hydrodynamic sizes were obtained by cumulative analysis of autocorrelation data. Zeta-potential values were obtained from electrophoretic mobility values using the Smoluchowski approximation.

2.6.3. Atomic force microscopy (AFM): The changes in morphology and roughness of the multilayers and were followed using AFM. AFM imaging of the multilayers was performed using Veeco MultiMode V instrument in dynamic mode.

2.6.4. Magnetic force microscopy (MFM): To obtain information about magnetic properties of iron oxide nanoparticle containing multilayers, MFM was performed using Veeco MultiMode V instrument. Magnetized tip was used under tapping mode.

2.6.5. Fourier Transform Infrared (FTIR) Spectroscopy: Fourier transform infrared (FTIR) spectrum of iron oxide nanoparticles was recorded using a ThermoScientic FTIR instrument (Nicolet iS10). Magnetic nanoparticles were freeze-dried prior to measurement.

2.6.6. X-ray Diffraction: To characterize crystallinity and obtain structural information about the iron oxide particles, XRD analysis of freeze-dried iron oxide nanoparticles was performed using Rigaku X-Ray Diffraction (Model, Miniflex) with CuKα (30 kV, 15 mA, λ = 1.54051 ˚A). Freeze dried sample of iron oxide nanoparticles were used for measurement within 2 theta range of 20 – 90˚.

2.6.7. Transmission Electron Microscopy (TEM): A drop of iron oxide nanoparticle solution was placed on a surface of copper grid coated with carbon substrate with 3 mm diameter. After deposition of the iron oxide nanoparticles at the surface, samples were air-dried. Transmission electron microscopy (TEM) images were obtained using FEI Tecnai G2 within the voltage range of 20-120 kV.

CHAPTER 3

RESULTS AND DISCUSSION

3.1. Characterization of magnetic iron oxide nanoparticles:

3.1.1. Structural characterization:

For the structural analysis of iron oxide nanoparticles Fourier Transform Infrared Spectroscopy (FTIR) and XRD analyses were performed (Figure 3.1 and Figure 3.2, respectively).

The broad peak observed at 3400 cm^{-1} is associated with the –OH stretching band of the hydroxyl groups of water molecules. It is also possible that some water molecules remained adsorbed at the surface of the particles and –OH stretching band of the hydroxyl groups of water also appear at the same place. The peak observed at 1598 cm^{-1} is related to -OH deformation modes of hydroxyl groups of ammonium hydroxide and water molecules. Also a peak is observed at 550 cm^{-1} corresponding to Fe-O bonds, hence proving the presence of iron oxide particles. Also the peaks at 1029 cm^{-1} and 820 cm^{-1} belong to the Fe-OH vibrations. Fe-OH and Fe-O vibrational peaks confirm the presence of iron oxide nanoparticles. Our results are in good agreement with the FTIR spectra of magnetite nanoparticles previously reported in the literature [152, 153, 154, 155].
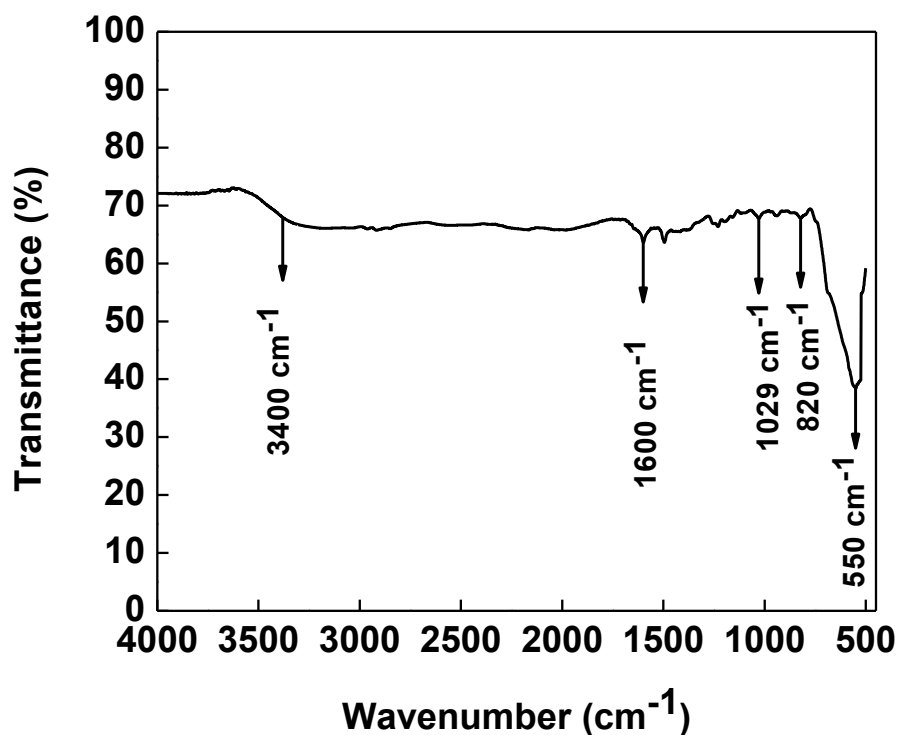
Figure 3.1 FTIR spectrum of iron oxide nanoparticles.

To characterize crystallinity and obtain structural information about the iron oxide particles, samples were analyzed by XRD. As seen in the XRD pattern (Figure 2), the iron oxide particles had 6 diffraction peaks at 2θ of 30, 35.6, 43, 53.5, 57, and 63 representing the corresponding [220, 311, 400, 422, 511, 440] planes of Fe_3O_4 crystals, respectively. This indicates the presence of magnetite phase of iron oxide particles with spinel structure [156]. Note that the peaks for maghemite particles (γ-Fe_2O_3), i.e. (110), (210) and (211) were not recorded [157]. The XRD patterns were in good agreement with XRD patterns of magnetite phase of iron oxide which were previously reported in the literature [154, 158, 159]. Scherrer Equation was used to estimate the mean particle size. The mean particle size was calculated as 9.27 nm.
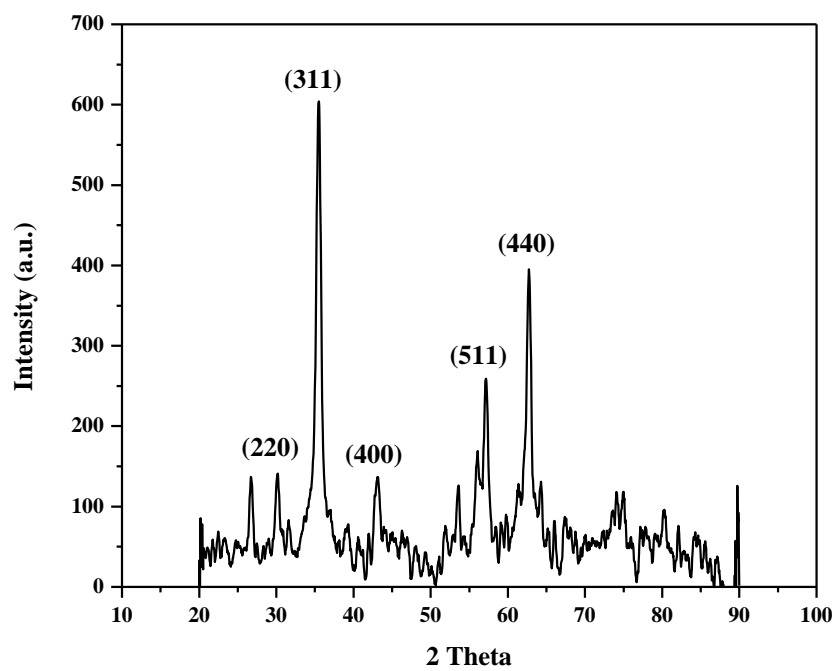
Figure 3.2 XRD pattern of iron oxide nanoparticles.

3.1.2. Particle size analysis:

Morphological and size characterizations were performed using transmission electron microscopy (TEM). Figure 3.3 shows TEM images of iron oxide nanoparticles synthesized via co-precipitation technique using ultrasonication.
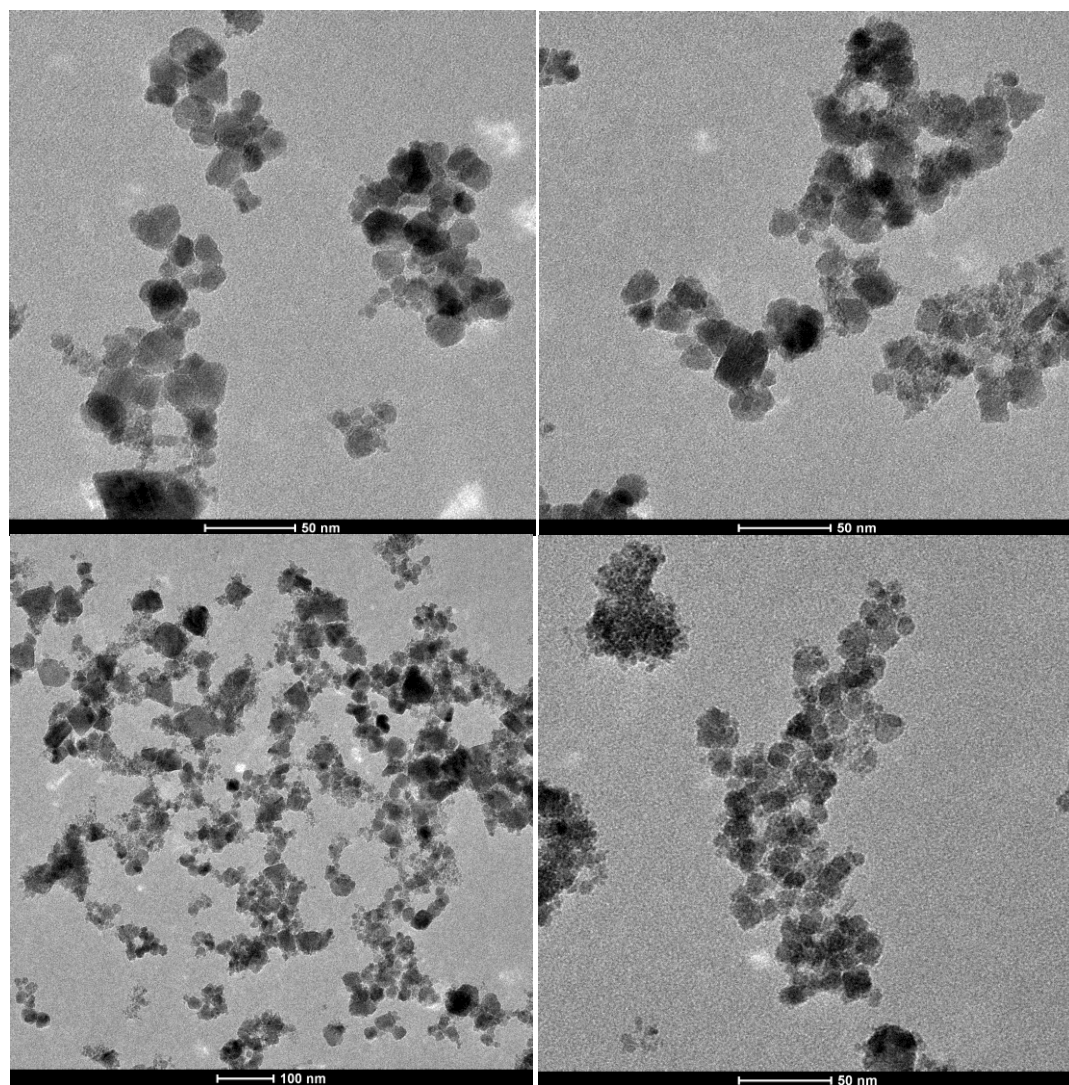
Figure 3.3 TEM images of magnetite nanoparticles synthesized via ultra-sonication technique.

As seen in Figure 3.3, most of the particles had spherical shape. The diameter of the particles varied between 9 nm and 26 nm. The maximum size even for the agglomerated particles was recorded to be ~26 nm. For a more detailed particle size analysis via TEM imaging, we used Image J software. The average particle size of the particles as depicted by the histogram (Figure 3.4) was found to be 8 ± 1.5 nm (Standard Deviation (σ) = 18%). S. Szunerits et al. has also followed a similar synthesis procedure. They reported the particle size as 25 ± 1.5 nm ($\sigma = 6\%$). Although we succeeded to synthesize smaller particles, our particles exhibited slightly less mono-dispersity. The reason for obtaining smaller particle size might be a difference in the experimental procedure. In contrast to Szunerits [160], refluxing system was used in our experiments to prevent the evaporation of the solvent during the synthesis of iron oxide nanoparticles. This might have decreased the dipolar attraction among the iron oxide nanoparticles and provided particles with smaller size.
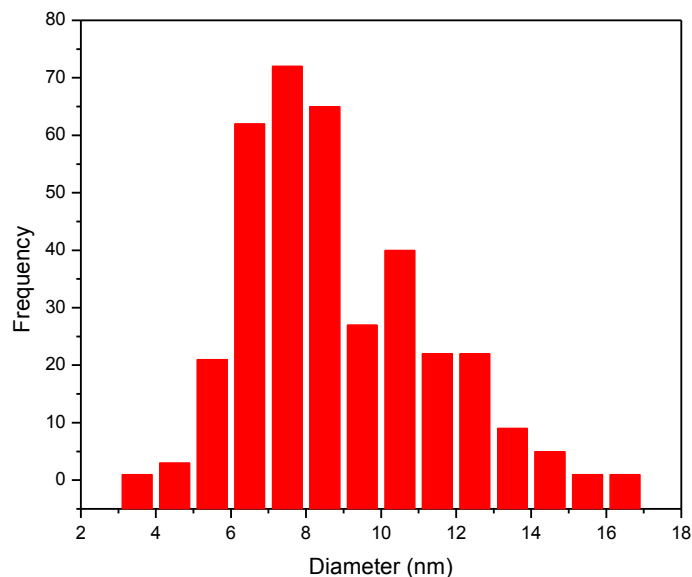
Figure 3.4 Particle size histogram for the TEM images of magnetite nanoparticles using Image J software.

Particle size measurements were also performed using dynamic light scattering (DLS) technique. The number average particle size recorded by DLS (Figure 3.5) was found to be 40 ± 13.8 nm ($\sigma = 34.5\%$). Standard deviation was measured using standard deviation formula.

$$\sigma = \sqrt{\frac{1}{N}\sum_{i=1}^{N}(x_i - \mu)^2}$$

where,

σ is standard deviation,

N is the total number of measurements

x_i is a measurement

μ is the arithmetic mean of the measurements
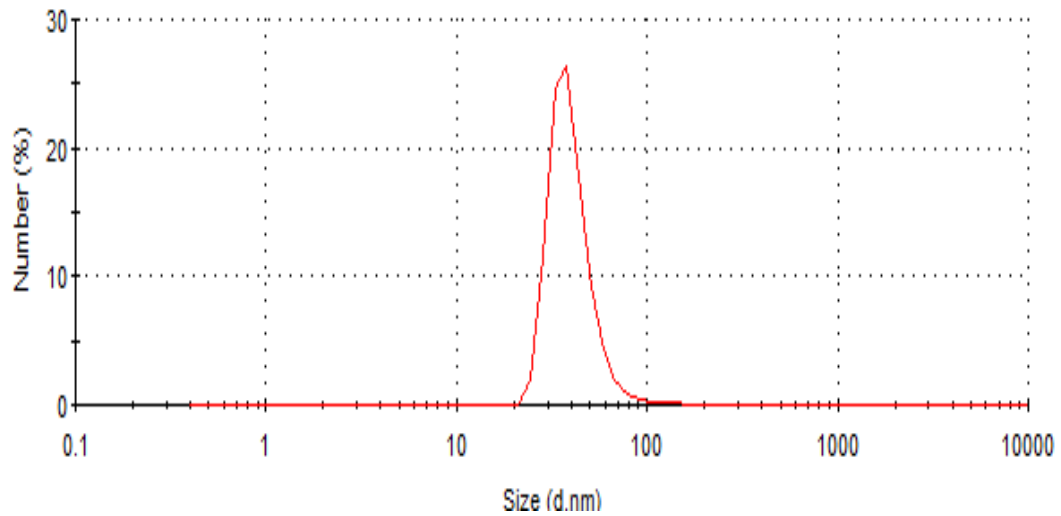
Figure 3.5 Number average hydrodynamic size distribution of iron oxide nanoparticles by DLS.

Comparing the DLS and TEM measurements, a clear difference in the size was observed. This is because DLS measures hydrodynamic diameter, whereas TEM provides information about the projected area diameter. In other words, hydrodynamic diameter determines the size of the particle together with the solvent layer attached to it, while TEM imaging provides information only about the particle since there is no hydration layer. Another reason for obtaining higher particle size via DLS is the enhanced aggregation of the magnetic nanoparticles in aqueous environment due to their magnetic nature leading to dipolar attraction among the particles.

3.1.3. pH stability of iron oxide nanoparticles:

The pH of the solution was found to be 4 right after the synthesis and the zeta-potential was recorded as +40.85 ±2.11 mV. The electrostatic repulsion among the iron oxide nanoparticles provided colloidal stability in aqueous solution for more than 24 hours. Figure 3.6 shows evolution of number average hydrodynamic size as a function of time.

pH-stability of the magnetite particles was followed by measuring the hydrodynamic size and zeta-potential of the particles as a function of pH (Figure 3.7A and 3.7B). To examine the pH-stability, two different samples were used. The pH of the solution containing iron oxide nanoparticles was either increased above pH 4 or decreased below pH 4. Note that the pH of the solution after synthesis was recorded to be ~ 4. As seen in Figure 3.7A, hydrodynamic size increased above pH 4 and showed a sharp jump above pH 5 indicating the aggregation of the particles and loss in aqueous solution stability. Aggregation of the particles can be correlated with the decrease in zeta-potential of the particles as the pH was increased. When the pH was gradually decreased below pH 4, a decrease in the zeta-potential of the magnetite particles was also recorded. Although the zeta-potential decreased down to +18.95±4.9 mV at pH 3, colloidal stability was not affected. No significant change in hydrodynamic size was recorded at pH 3. Further decreasing pH below 3 resulted in instantaneous precipitation of the particles. The

isoelectric point was determined to be at pH 6.8 by linear interpolation of the data. These results suggest that the workable range with magnetite particles was between pH 3-4. The results were observed were in agreement with the literature [161].
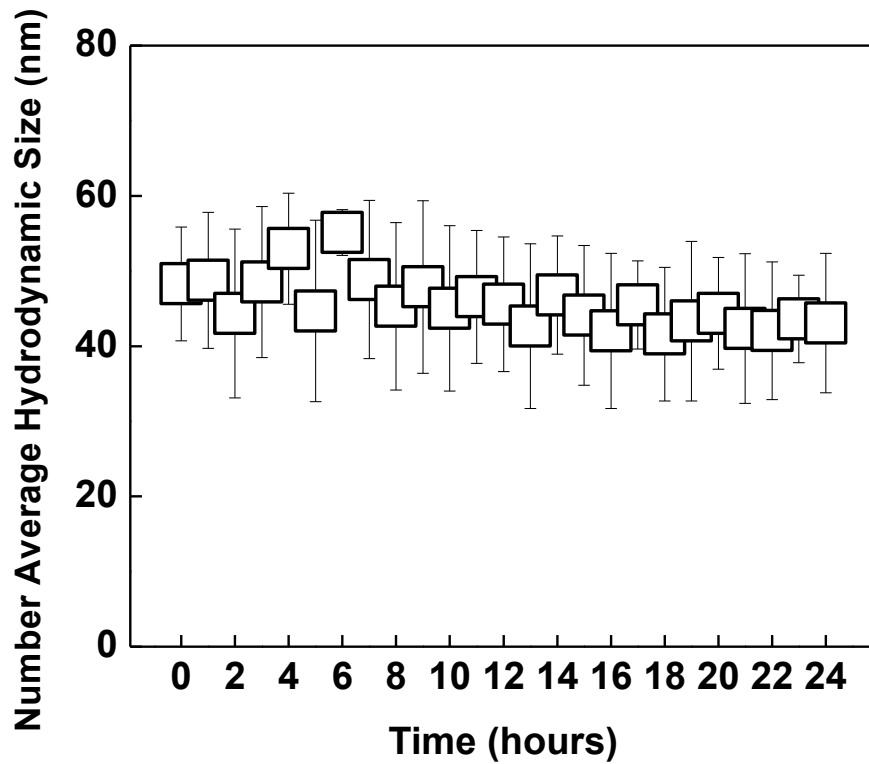
Figure 3.6 Evolution of number average hydrodynamic size of iron oxide nanoparticles as a function of time.
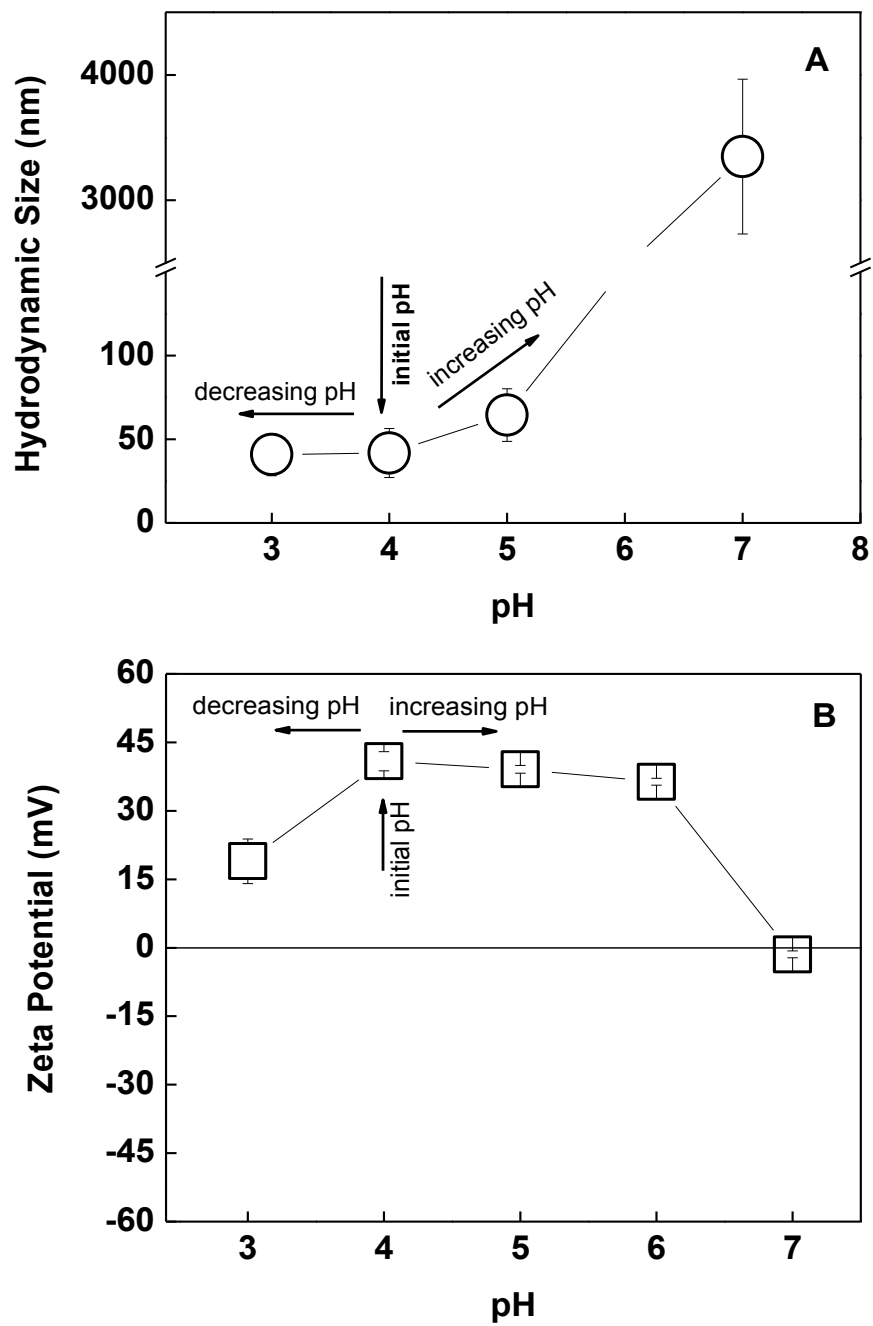
Figure 3.7 Hydrodynamic size and zeta-potential of iron oxide nanoparticles as a function of pH.

3.2. Characterization of the multilayers:

3.2.1. Layer-by-Layer growth of the films:

As mentioned in Section 3.1.2, magnetite nanoparticles were stable in a very narrow pH range. Therefore, multilayers were fabricated at pH 4 - the pH at which magnetite particles showed the highest pH-stability in the long term - to avoid the precipitation of the particles during film assembly process. PVCL and TA were chosen as the polymer building blocks of the films. Multilayers were constructed in the following order: 1) TA; 2) PVCL; 3) TA; 4) Magnetite nanoparticles and this cycle was repeated until desired number of layers were deposited at the surface. Figure 3.8 shows schematic representation of the multilayer architecture. These 4 layers will be denoted as 1 tetralayer in the rest of the thesis.
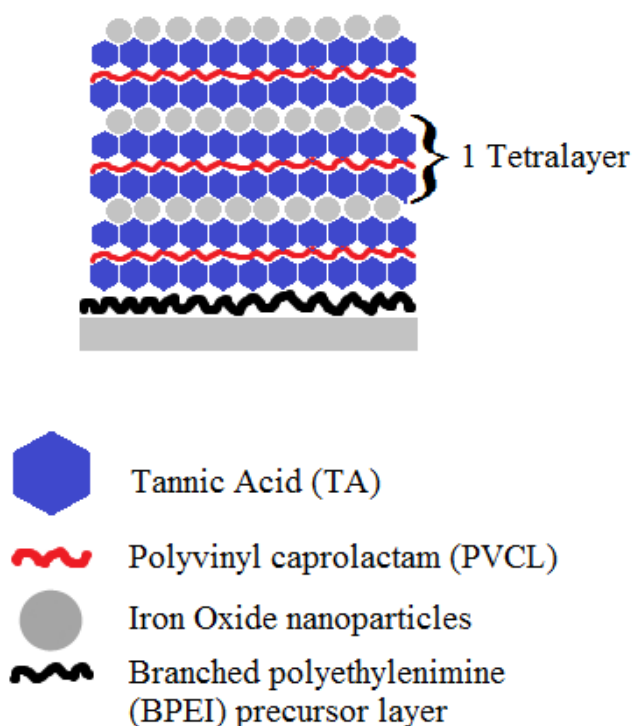
Figure 3.8 Multilayer architecture.

PVCL is a neutral polymer and has hydrogen accepting carbonyl groups. TA is a polyphenol with 25 hydroxyl groups per molecule which may act as hydrogen donors. TA has a pK_a of 8.5. At the deposition pH of 4, TA has most of its hydroxyl groups in the protonated form. Therefore, the driving force for deposition of PVCL onto TA layer is hydrogen bonding interactions. In contrast, the driving force for the deposition of positively charged magnetite particles onto TA layer is electrostatic interactions. Note that ionization of TA is enhanced even at pH 4 when exposed to positively charged iron oxide nanoparticle solution, resulting in an increase in the number phenolate ions. Enhanced ionization of polyacids in the presence of salt cations [162] and/or polycations [98] has been reported earlier.

Film growth was followed using UV-Vis Spectroscopy. Multilayers were constructed on quartz slides and the change in intensity of the peak centered at 220 nm was followed as a function of number of TA layers. Note that pure TA solution exhibits 2 peaks centered at 219 nm and 276 nm in its neutral form (Figure 3.9A inset) [163]. As seen in Figure 3.9A, the intensity of the peak at 220 nm was increased with increasing number of TA layers, indicating successful growth of the film. When the intensity of the peak at 220 nm is plotted as a function of TA layer number, a linear growth profile is obtained for the multilayers (Figure 3.9B). In contrast to TA, PVCL and iron oxide nanoparticles do not show absorbance in the UV-Vis region. However, the absorbance of the multilayer films progressively increased between 300 nm and 600 nm with increasing number of layers, indicating the successful growth of the film.
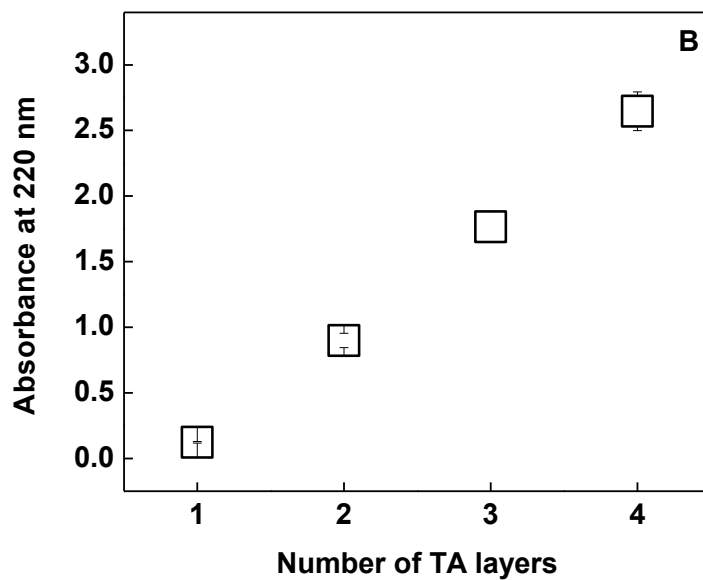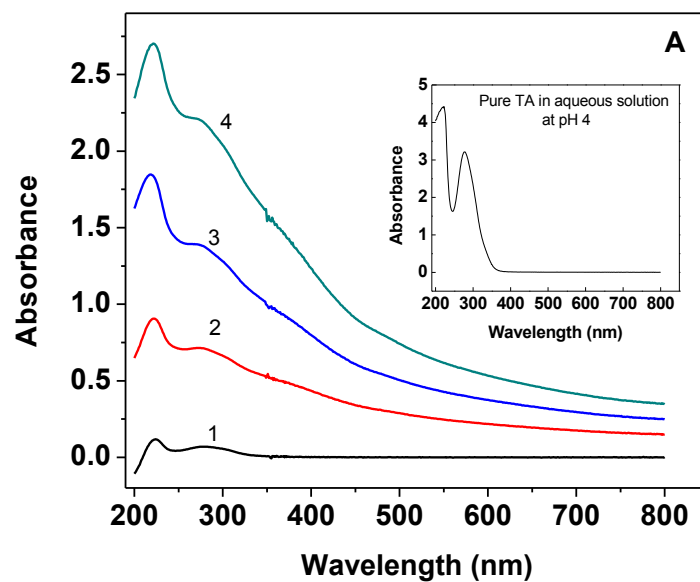
Figure 3.9 UV-vis spectrum of multilayers after TA deposition after every tetralayer (Panel A). Intensity of the peak centered at 220 nm vs number of TA layers after every tetralayer (Panel B).

Multilayer growth was also confirmed by thickness measurements using AFM. Figure 3.10 shows evolution of film thickness obtained via AFM with increasing number of tetralayers. Different from the data obtained via UV-Vis Spectroscopy, a deviation from linearity was recorded at the end of 4th tetralayer. This is probably due to significant increase in surface roughness and enhanced aggregation of iron oxide nanoparticles at higher number of layers, making film surfaces inhomogeneous and leads to unreliable thickness measurements via AFM.
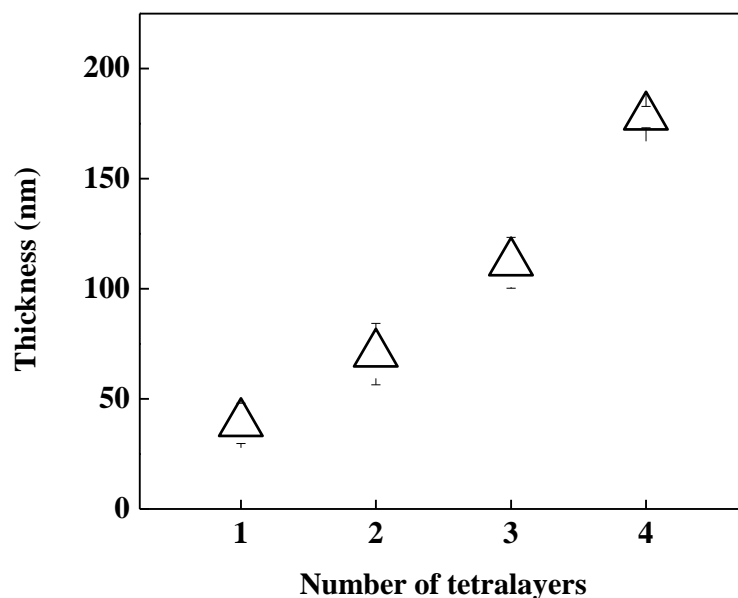
Figure 3.10 Evolution of film thickness with increasing number of tetralayers via atomic force microscopy (AFM).

To further examine the change in morphology and surface roughness of the multilayers with increasing number of tetralayers, topographical view of the multilayers were obtained. Figure 3.11 shows AFM height images of the multilayers composed of 1, 2, 3 and 4 tetralayers. As visually observed in the images, surface roughness increases with

increasing number of layers. Figure 3.11E shows the change in roughness values with increasing number of layers. The increase in surface roughness can be explained by higher interpenetration of the layers as moving away from the substrate. Increase in surface roughness also resulted in enhanced aggregation of iron oxide nanoparticles at the surface. The aggregation as well as the increment in the number of iron oxide nanoparticles were remarkable at higher number of layers which was evident by the clusters of iron oxide nanoparticles observed in the images (Figure 3.11D). In addition to increasing surface roughness, another reason behind the aggregation of the iron oxide nanoparticles at the surface is the enhanced attraction among the iron oxide nanoparticles due to the dipolar attractions as the amount of iron oxide nanoparticles increase within the multilayers with increasing number of tetralayers. Decher et al. [139] also showed that aggregation of the magnetic nanoparticles and surface roughness increase with increasing number of layers in case of electrostatic multilayers of polyallylamine hydrochloride (PAH) and polystyrene sulfonate (PSS) containing iron oxide nanoparticles.
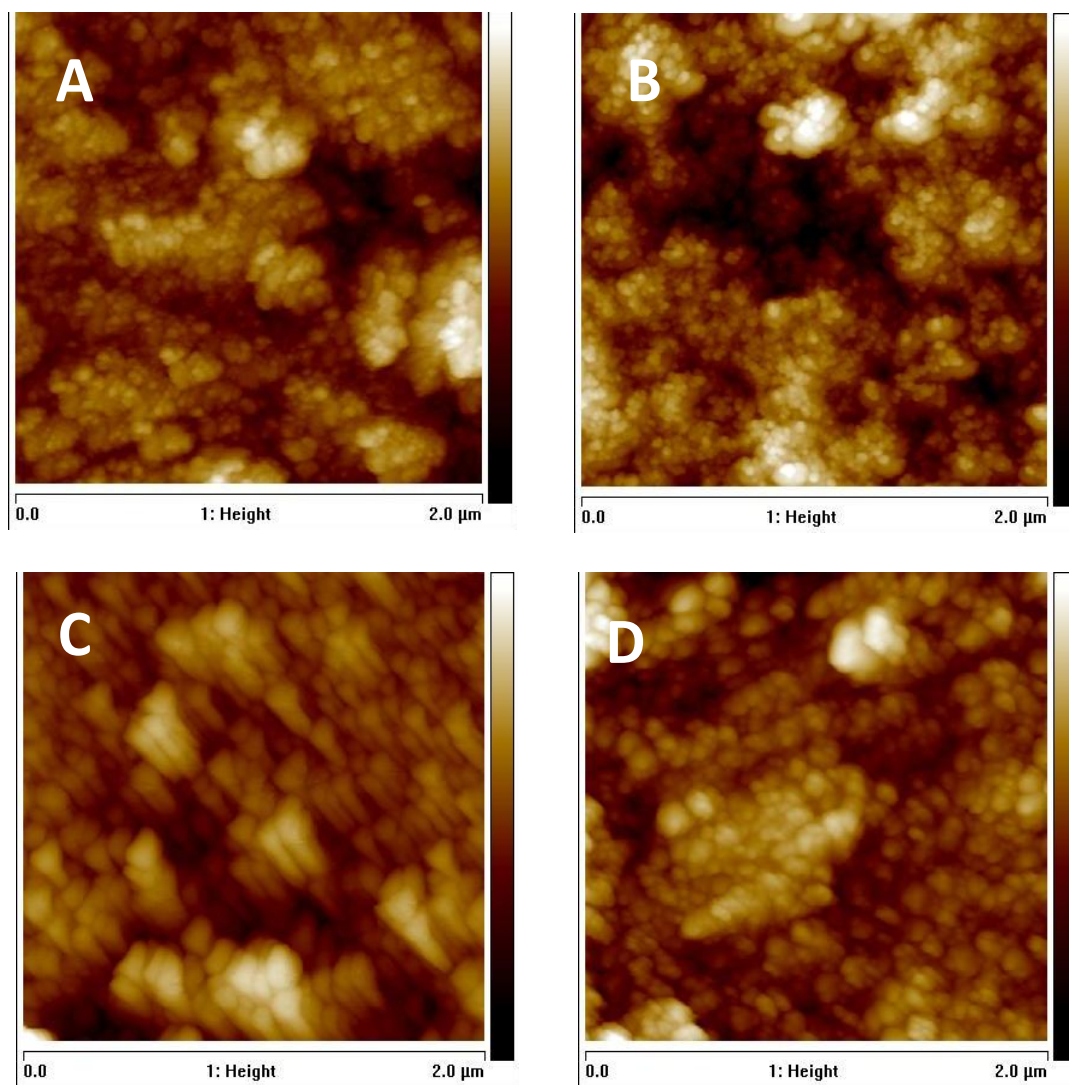
Figure 3.11 Atomic force microscopy images of 1 tetralayer (Panel A); 2 tetralayers (Panel B); 3 tetralayers (Panel C); 4 tetralayers (Panel D) of multilayers of TA, PVCL and iron oxide nanoparticles. Panel E shows evolution of surface roughness with increasing number of layers.
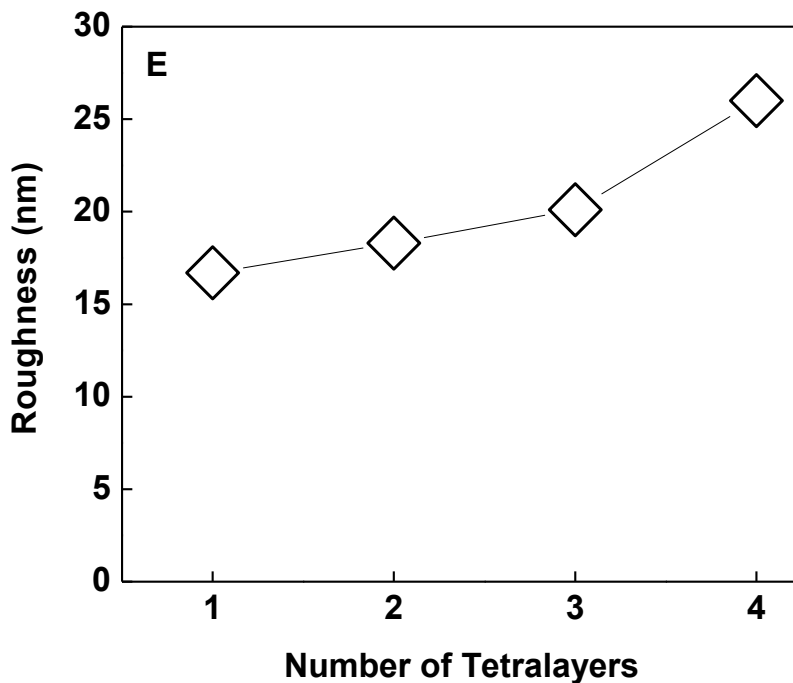
Figure 3.11 Continued.

3.2.2. Characterization of magnetic properties of the multilayers:

Magnetic force microscopy measurements were carried out to prove the magnetic properties of the iron oxide nanoparticles within the multilayer films. Magnetic force microscopic measurements were performed using a special tip which was magnetized prior to measurements to provide interaction with the magnetic field of the multilayer films. At each measurement, scan line was consisted of 2 passes, i.e. trace and re-trace. In the first scan, the topographical image was obtained in the tapping mode (tracing and re-tracing the surface topography). Then, the tip is raised up to a certain distance (~ 16 nm) and a second pass (trace/re-trace cycle) was carried out. The lift mode minimized the influence of surface topography and allowed measuring magnetic interactions. In

other words, magnetic interactions were detected during the second pass [170-172]. To confirm the magnetic properties of multilayers containing iron oxide nanoparticles, we first contrasted MFM phase images (Figure 3.12) of a 1-bilayer film containing tannic acid and polyvinyl caprolactam but no iron oxide nanoparticles (Panel A) and 1 layer of iron oxide nanoparticles (Panel B).
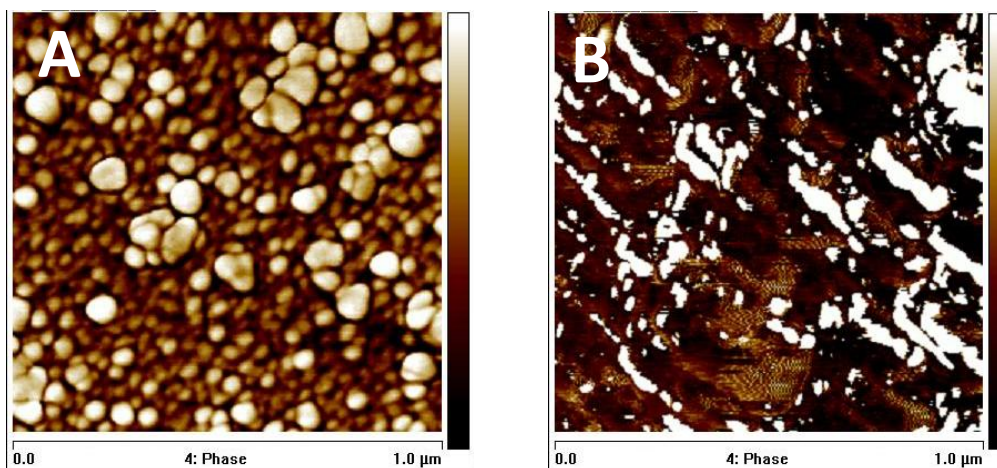
Figure 3.12 MFM phase images of 1-bilayer pure polymer film of tannic acid (TA) and polyvinyl caprolactam (Panel A) and 1 layer of iron oxide nanoparticles (Panel B).

As seen in Figure 3.12, only polymeric lumps could be observed on the surface of the multilayers containing no iron oxide nanoparticles. On the other hand, light and dark regions were observed on the surface of a 1 layer of iron oxide nanoparticles. The difference between the 2 phase images arises from dipolar effect, observed in the layer containing iron oxide nanoparticles. Magnetic nanoparticles have two poles, i.e. north and south pole. The tip was also magnetized with either of the poles, i.e. north or south during magnetization. When the tip interacts with the similar pole on the surface, it repels the surface and a lighter region on the surface is observed. The darker region is observed due attraction of the tip and particles on the surface.

Figure 3.13 shows the phase images of 1-, 2-, 3- and 4- tetralayer films. In Figure 3.13A, the film contained only 1 layer of iron oxide nanoparticles and the dipolar effect of the magnetic iron oxide nanoparticles can be clearly observed by the contrast of the light and dark regions. However, further depositing tetralayers at the surface resulted in a significant increase in the amount of lighter regions (Figure 3.13D) and the contrast of the lighter and darker regions could no longer be observed. Couple of suggestions can be made for this phenomenon:

1) Alignment of the iron oxide nanoparticles is affected by the alignment of the previously deposited iron oxide nanoparticles which would induce the appearance of either the lighter or darker regions at the surface. For example, if the number of iron oxide nanoparticles facing the tip with a similar pole is higher in number than that facing the tip with an opposite pole, then the formation of lighter regions on the surface will be induced. This is the case observed in Figure 3.13D. However, the opposite case might also be possible resulting in formation of darker regions. Both cases would result in an increase in the contrast of dark and light regions.

2) The tip used during MFM measurements is capable of interacting with the iron oxide nanoparticles which are maximum 100 nm beneath the top of the film. This means that the interaction of the tip with the topmost iron oxide nanoparticles might be affected by the iron oxide nanoparticles which were deposited previously into the multilayers. The tip interacts with higher number of iron oxide particles as the number of tetralayers at the surface increases. If the total number of iron oxide nanoparticles which interacts with the tip with a similar pole is greater than that which interacts with the tip with an opposite mole, the enhanced repulsion among the nanoparticles and the tip would result in formation of larger amount of lighter regions.

3) The increase in surface roughness with increasing number of tetralayers resulted in deposition of higher amount of iron oxide nanoparticles at the surface. However, higher number of iron oxide nanoparticles at a particular layer might have induced aggregation

of the iron oxide nanoparticles at the surface through the lateral position due to stronger dipolar effect as the distance between the iron oxide nanoparticles gets shorter. This enhanced dipolar affect among the aggregated nanoparticles could be another reason of the repulsion between the tip and the iron oxide nanoparticles resulting in an increase in the lighter domains.

In conclusion, MFM images fortify the presence of higher amount of iron oxide nanoparticles at the surface as the number of layers of iron oxide nanoparticles increase. However, no matter how the iron oxide nanoparticles align within the multilayers, the contrast of the light and dark regions will be lost with increasing number of iron oxide layers. Therefore, MFM may not be a proper technique to characterize magnetic properties of the multilayer films with more than one layer of iron oxide nanoparticles. Further analysis of the multilayers will be performed using MFM to scrutinize the convenience of the technique for characterization of magnetic properties of ultra-thin polymer multilayer films containing more than one iron oxide layers.
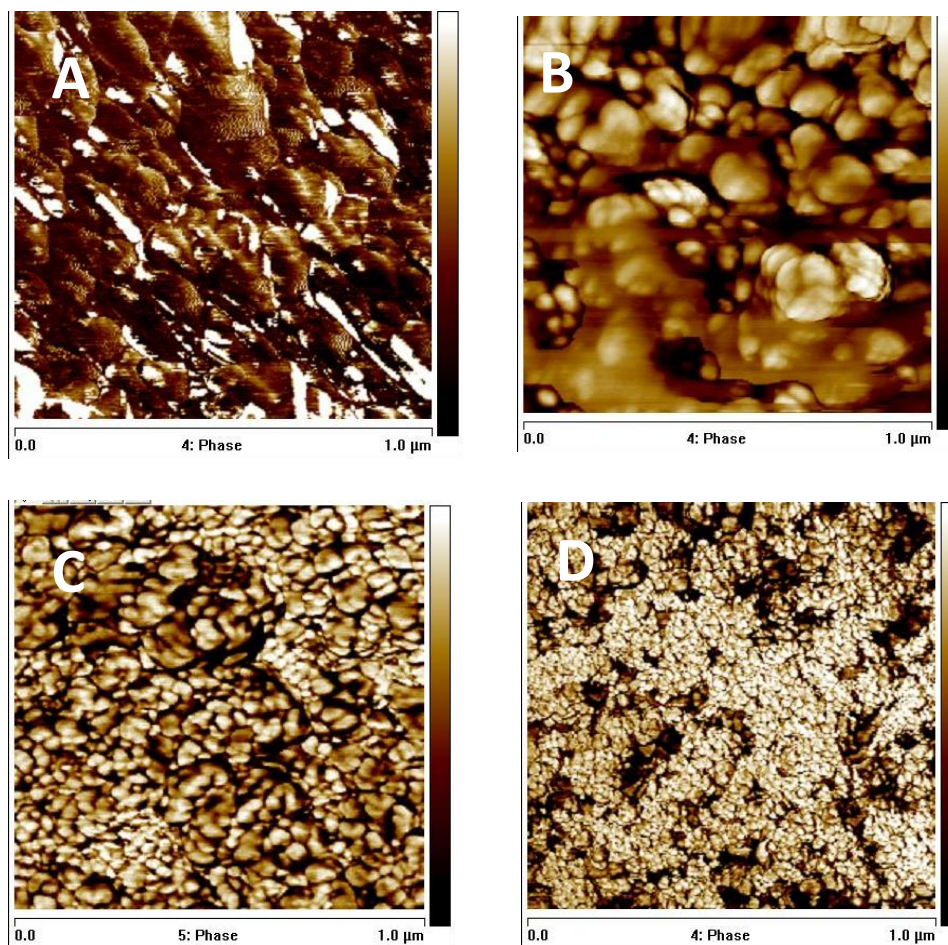
Figure 3.13 MFM images of 1tetralayer-(Panel A); 2tetralayer- (Panel B); 3tetralayer-
(Panel C) and 4tetralayer- (Panel D) films.

3.2.3. pH stability:

pH stability of the multilayers was determined by immersing the multilayers into buffer
solutions at different pH values for 30 minutes and then tracking the amount of material
remained at the surface using UV-vis Spectroscopy. As mentioned in the experimental
section, the multilayers were prepared at pH 4.0. pH stability was evaluated by

immersing the films to either lower or higher pH values. Figure 3.14A shows the change in intensity of the peak centered at 220 nm as the acidity increased. Almost no change in peak intensity was recorded indicating the stability of the multilayers. Similarly, no significant change in the intensity of the peak was recorded when the pH was gradually increased from pH 4 to pH 9 (Figure 3.14B). To further understand the effect of iron oxide nanoparticles on the pH-stability of the multilayers, pH-stability of pure PVCL and TA multilayers which was constructed at pH 4 was also examined. Filled squares (in Figure 3.14B) show the change in the normalized absorbance at 220 nm for PVCL/TA layers (in the absence of iron oxide nanoparticles). As seen in Figure 3.14B, incorporation of iron oxide nanoparticles within the multilayers did not cause a significant change in the pH-stability of the multilayers. Therefore, it can be concluded that the stability of the multilayers against pH was mostly due to nature of the association among the polymer building blocks.
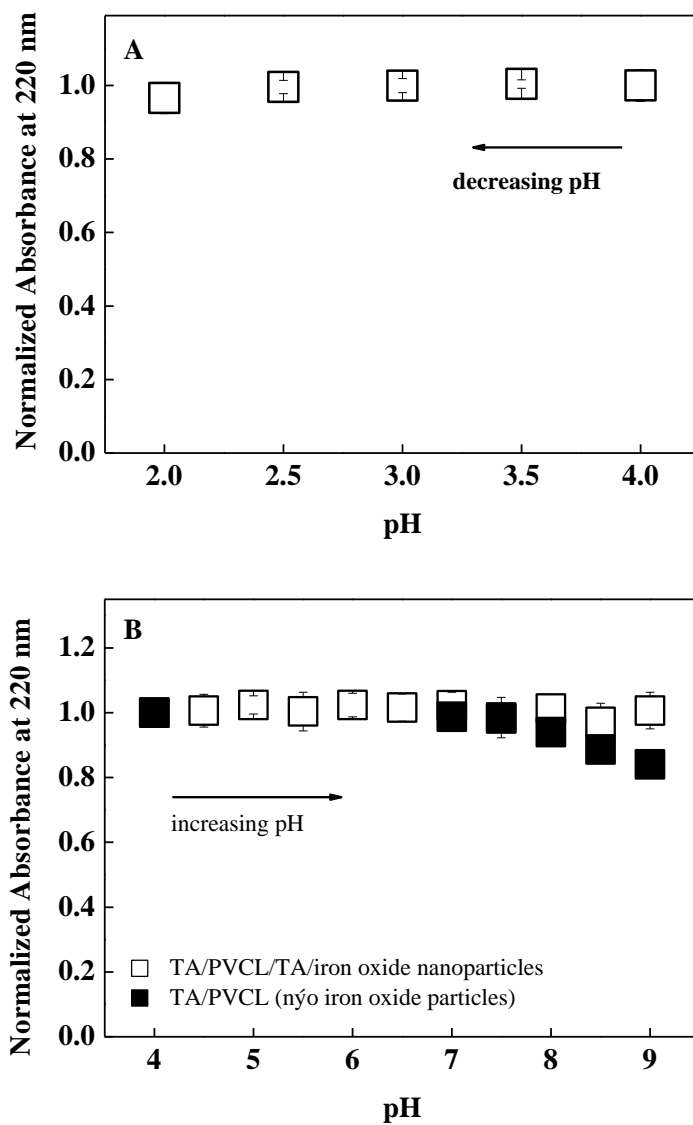
Figure 3.14 pH stability of multilayers of TA/PVCL/TA/iron nanoparticles at decreasing (Panel A) and increasing (Panel B) pH values. Filled squares show the pH-stability of pure polymer multilayers (TA/PVCL constructed at pH 4) as the acidity was decreased and is plotted for comparison.

The stability of the multilayers has also been checked by following the change in the UV-visible spectra of multilayers between 300 and 600 nm at different pH values. Remember that the peak centered at 220 nm belongs to TA. Neither PVCL nor iron oxide nanoparticles has a peak between 200 nm and 800 nm. However, the absorbance of the multilayer films progressively increased between 300 nm and 600 nm as the number of iron oxide nanoparticle layers increased within the multilayers. Therefore, contrasting the UV-Visible spectra of the multilayers at different pH values could provide information about the retention of iron oxide nanoparticles at the surface. Figure 3.15 shows the UV-Visible spectrum of the multilayers at pH 4, pH 6, and pH 9. As seen in Figure 3.15, no significant change in the UV-Visible spectra of multilayers were recorded, indicating also the retention of iron oxide nanoparticles within the multilayers.
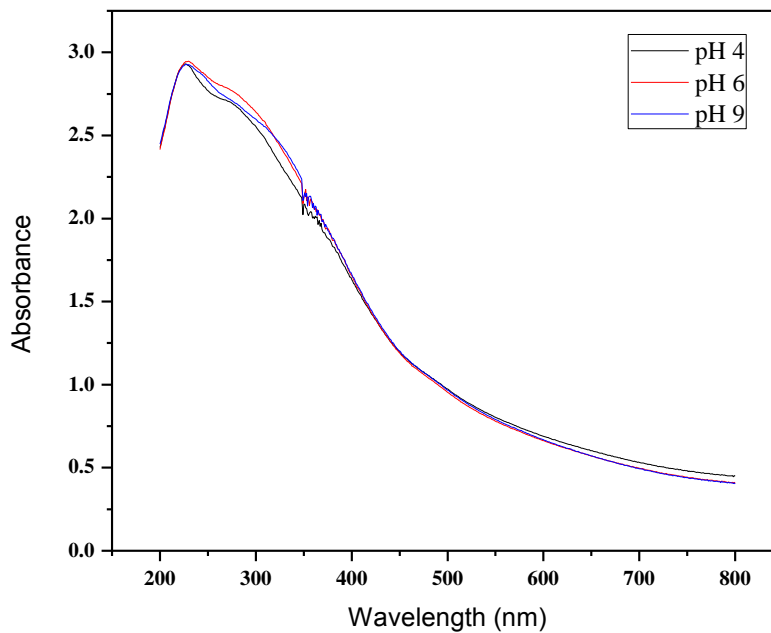
Figure 3.15 UV-Vis spectra of multilayers at pH 4, pH 6 and pH 9.

Changes in morphology of the multilayers with decreasing or increasing pH have also been examined using AFM. AFM images (figure 3.16) show that roughness of the films did not show a significant change when the multilayers were exposed to pH 2. In contrast, when the multilayers were exposed to pH 7.5 for 30 minutes, films became rougher due to increased ionization of TA resulting in partial disruption of the hydrogen bonds among PVCL and TA molecules and loosening of the film structure.

pH 2 **pH 4** **pH 7.5**

R_a = 15 nm R_a = 15.2 nm R_a = 28.9 nm
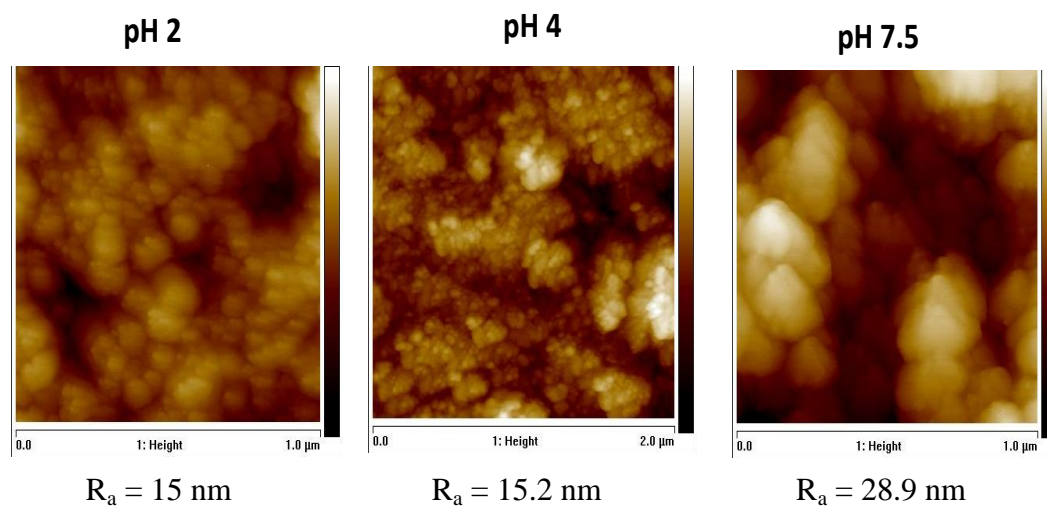
Figure 3.16 AFM images of 4 tetralayers of TA/PVCL/TA/iron oxide nanoparticles after exposure to pH 2 and pH 7.5 for 30 minutes. AFM image of the multilayers which were constructed at pH 4 was plotted for comparison.

Multilayers of TA/PVCL/TA/iron oxide nanoparticles have also been examined using MFM (Figure 3.17). As seen in the MFM images, we did not observe a significant difference in MFM images of the films at pH 4 and pH 2. In contrast, we have a decrease in the amount of lighter regions. This could be due to loosening of the multilayer structure with increasing pH which might have resulted in a decrease in the interaction among the iron oxide nanoparticles.
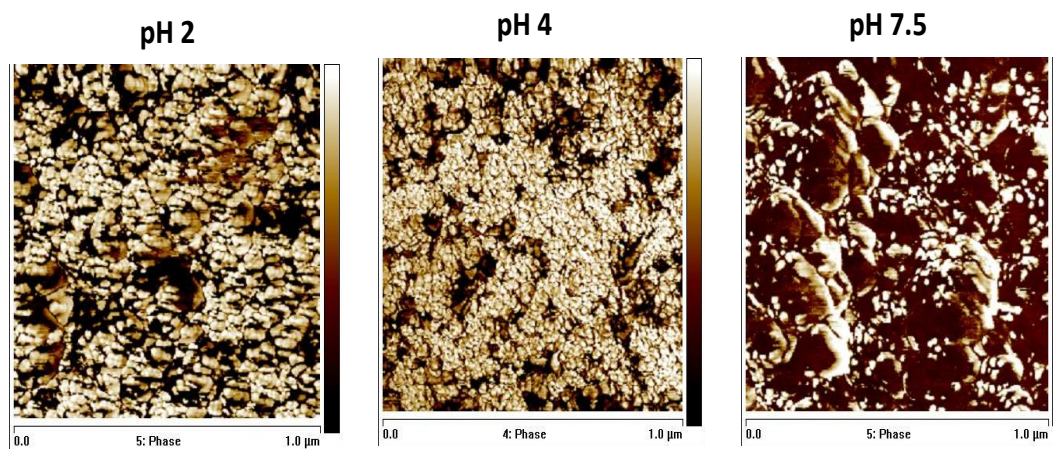
Figure 3.17 MFM images of 4 tetralayers of TA/PVCL/TA/iron oxide nanoparticles after exposure to pH 2 and pH 7.5 for 30 minutes. MFM image of the multilayers which were constructed at pH 4 was plotted for comparison.

3.3. Controlled release of ciprofloxacin from multilayers:

In this part of the study, potential of multilayers were examined for their controlled release properties at physiologically related pH values and temperature.

CIPRO was loaded into the multilayers during film preparation process (Figure 3.18). CIPRO has a two pK_a values, the first one is 6.43 [167, 168, 169] and the second is 8.68 [167, 168, 169]. At the multilayer deposition pH of 4, CIPRO is positively charged, whereas TA is partially negatively charged. Thus, CIPRO and TA can interact with each other through electrostatic interactions. Complexes of CIPRO and TA were prepared in aqueous solution by simply mixing the CIPRO and TA solutions at certain molar ratios (details are given in experimental section). Then, multilayers were constructed by immersing the substrate into solutions following the order of (CIPRO+TA) complexes/PVCL/(CIPRO+TA) complexes/iron oxide nanoparticles. For release experiments, 15 tetralayer films were constructed on both sides of the glass slides.

Release experiments were followed at 2 different pH and temperature values, i.e. pH 7.5 at 25°C and 37°Cand pH 8.5 at 25°C and 37°C.
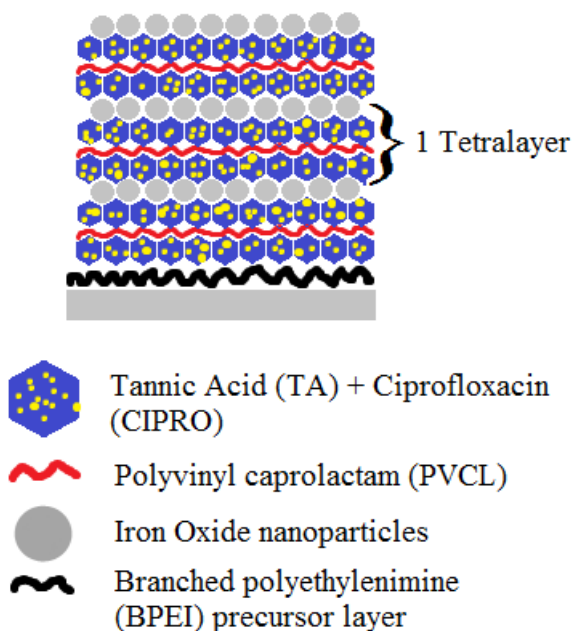
Figure 3.18 Architecture of ciprofloxacin loaded multilayers.

Prior to releasing CIPRO from the multilayers, aqueous solution of CIPRO was examined using UV-Vis Spectroscopy. To make sure that the peak centered at 270 nm belonged only to CIPRO, UV-Visible spectra of CIPRO and TA were contrasted at pH 7.5 and pH 8.5. As seen in Figure 3.19, CIPRO in aqueous solution has a peak centered at 270 nm and this peak does not overlap with any of the peaks of TA. Thus, for release experiments, the change in the intensity of the peak at 270 nm was monitored as a function of time. Figure 3.20 shows the normalized intensity of the peak centered at 270 nm as a function of time at pH 7.5 and pH 8.5 at 37°C.Note that once the release at pH

7.5 was complete, multilayers were immersed to pH 8.5 buffer solutions at the same temperature. As seen in Figure 3.20, multilayers release around half of the amount of CIPRO at pH 7.5. The reason is: 1) At pH 7.5, CIPRO is electrically neutral (first pK_a of CIPRO is 6.43) [167, 168, 169]. Thus, it loses its electrostatic interactions with TA and releases from the multilayers. At pH 8.5, CIPRO carries more negative charge and its release from the multilayers should be facilitated due to electrostatic repulsion between negatively charged TA and negatively charged CIPRO. Also, at neutral and basic conditions the binding strength among the layers are weakened due to ionization of TA and loss in hydrogen bonding interactions among PVCL and TA. As also observed in AFM images (Figure 3.16) in Section 3.2.3, multilayers go into morphological changes after exposure to neutral pH conditions resulting in rough and loosened multilayer structure. The morphological changes observed within the multilayer structure provides a pathway and facilitates the release of CIPRO from the multilayers. One more parameter which might have affected the release of CIPRO is the formation of voids within the multilayers at 38-40 °C due to the phase separation of PVCL above its LCST. Such a structure could have facilitated the release of CIPRO molecules from the multilayers. Note that Sukhushvili and co-workers [174] and Erel et al [175] have earlier reported on the enhanced release of functional molecules above the LCST of the hydrogen accepting polymer component of the multilayers.
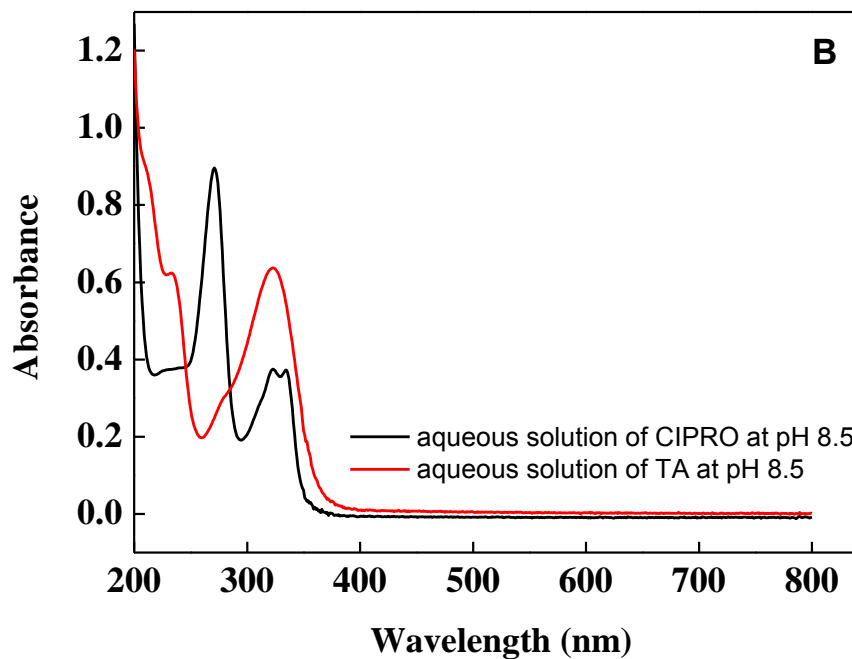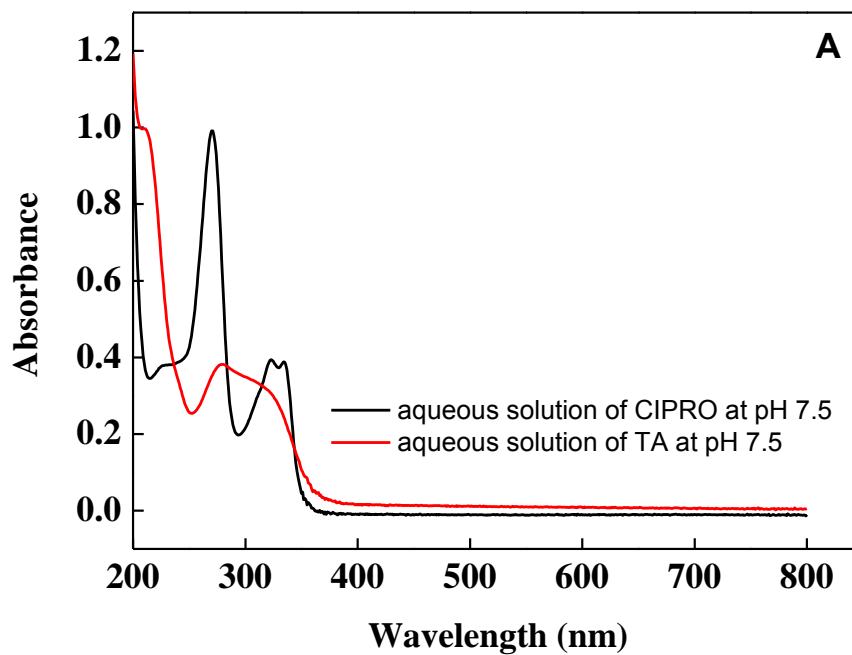
Figure 3.19 UV-Visible spectra of aqueous solutions of ciprofloxacin and TA at pH 7.5 (Panel A) and pH 8.5 (Panel B).
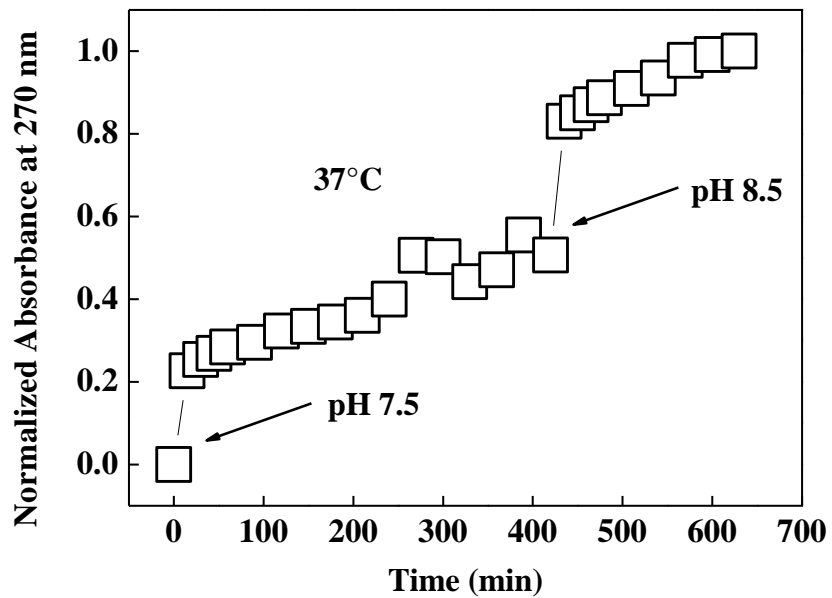
Figure 3.20 Release of ciprofloxacin from multilayers at pH 7.5 and pH 8.5 at approximately 37˚C.

CHAPTER 4

CONCLUSION AND OUTLOOK

Iron oxide nanoparticles with an average particle size of 9 nm (based on TEM imaging) were synthesized through ultrasound based co-precipitation. These iron oxide nanoparticles were successfully incorporated into temperature-responsive hydrogen-bonded polymer multilayers of PVCL and TA. Multilayers of PVCL, TA and iron oxide nanoparticles have been successfully constructed at pH 4 through hydrogen bonding interactions among PVCL and TA as well as electrostatic interactions among TA and iron oxide nanoparticles. Multilayers were highly stable at neutral and basic pH conditions. Magnetic properties of the multilayers were confirmed using MFM. It was also found that an antibiotic which is used for the treatment of different bacterial infections in the body, ciprofloxacin, can be successfully incorporated into the multilayers during film assembly and released from the multilayers simply by a pH trigger.

The work presented in this thesis can form a basis for the development of more advanced polymer platforms for bio-imaging and controlled release of functional molecules from surfaces. This study is also important for gathering a temperature-responsive polymer and iron oxide nanoparticles in the same polymer LbL film matrix. Therefore, these multilayers can be promising materials for future application as platforms for magnetothermally triggered release of functional molecules from surfaces.

The future work on this study will consist of the following parts:

1) Multilayers will be examined for magnetothermal trigger of drug molecules from the surface by applying AC magnetic field. An increase in temperature is expected to be induced within the multilayers after exposure to AC magnetic field followed by heating of iron oxide nanoparticles. Increase in temperature will probably induce conformational changes in the PVCL chains above the LCST. Such a conformational change in PVCL chain will probably result in formation of voids within the multilayers and release of drug molecules.

2) The multilayers presented in this thesis are capable of releasing the drug molecules at neutral and basic conditions, while retaining the iron oxide nanoparticles within themselves. It is also of interest to design multilayers which release both drug molecules and iron oxide nanoparticles simultaneously. Hydrogen-bonded multilayers which are capable of releasing both drug molecules and iron oxide nanoparticles will be designed.

REFERENCES

[1] C. Ankerfors, Polyelectrolyte Complexes: Their preparation, adsorption behavior, and effect on paper properties, *Licentiate Thesis, Royal Institute of Technology*, **2008.**

[2] S. L. Dakhara, C. C. Anajwala, *Syst. Rev. Pharm.*, **2010**, 1, 121-7.

[3] D. V. Pergushov, A. H. E. Muler, F. H. Schacher, *Chem. Soc. Rev.,* **2012**, 41, 6888-6901.

[4] V. V. Khutoryanskiy, *International Journal of Pharmaceuticals,* **2007,** 334, 15-26.

[5] S. Lankalopalli, V. R. N. Kolapalli, *Indian J. Pharm. Sci.*, **2009**, 71, 5, 481-487.

[6] R. M Fuoss, H. Sadek, *Science,* **1949,** 110, 552-554.

[7] A. S. Michaels, R. G. Miekka, *J. Phys. Chem.,* **1961,** 1765-1773.

[8] E. Tsuchida, K. Abe, *Advances in Polymer Science, Springer-Verlag, Berlin Heidelberg, Germany,* **1982,** 45, 1-130.

[9] V. Kabanov, *Multilayer Thin Films,* **2003**, Wiley-SCH Verlag GmbH, Weiheim, Germany, 47-86.

[10] V. A. Kabanov, A. B. Zenzin, *Pure Appl. Chem.,* **1984,** 56, 3, 343-354.

[11] M Senuma, S. Kuwabara, K. Kaeriyama, F. Hase, Y. Shimira, *J. Appl. Polym. Sci.,* **1986,** 31, 1687-97.

[12] Y. Hirouki, K. Takeshi, *Chem. Eng. Japan,* **1989,** 41, B11-5.

[13] J. G. Atkinson, *Biochem. Biophys. Acta.,* **1973,** 308, 41-52.

[14] Q. Zhao, Q. F. Sn, Y. Ji, J. Qian, C. Gao, *J. Membr. Sci.,* **2011,** 379, 19-45.

[15] H. Dautzenberg, J. Kotz, K. J. Linow, B. Phillipp, G. Rother, *Macromolecular complexes in chemistry and biology, Berlin, Springer Verlag,* **1994,** 119-33.

[16] P. Bertrand, A. Jonas, A. Laschewsky, R. Legras, *Macromol. Rapid Commun.*,**2000**, 21, 319–348.

[17] Z. Y. Tang, Y. Wang, P Podsiadlo, N. A.Kotov, *Adv. Mater.*, **2006**, 18, 3203–3224.

[18] R. K. Iler, *J. Colloid and Interface Sci.,* **1966**, 21,569-594.

[19] M. M. Viliers, D. P. Otto, S. J. Strydom, Y. M. Lvov, *Advanced Drug Delivery Review*s, **2011**, 63, 701-715.

[20] Y. Jang, S. Park, K. Char, *Korean J. Chem. Eng.,* **2011**, 28, 1149-1160.

[21] F. M. Koehler, M. Fabian, M. Rossier, M.Waelle, E. K. Athanassiou, L.K. Limbach, R. N. Grass, D. Gunther, W. J. Stark, *Chem. Commun.,* 2008, 32, 4862-4865.

[22] J. B. Schlenoff, S. T. Dubas, T. Farhat, *Langmuir,* **2000**, 16, 26, 9968-9969.

[23] A. Izquierdo, S. S. Ono, J. G. Voegel, P. Schaaf, G. Decher, *Langmuir,* **2005,** 21, 16, 7558-7567.

[24] P. A. Chiarelli, M. S. Johal, D. J. Holmes, J. L. Casson, J. M. Robinson, H. L. Wang, *Langmuir,* **2002,** 18, 1, 168-173.

[25] P. Bertrand, A. Jonas, A. Laschewky, R. Legras, *Macromol. Rapid Commun.,* **2000,** 21, 319-348.

[26] Z. Y. Tang, Y. Wang, P. Podsiadlo, N. A. Kotov, *Adv. Mater.,* **2006**, 18, 3203-3224.

[27] J. F. Quinn, A. P. R. Johnston, G. K. Such, A. N. Zeliktin, T. Caruso, *Chem. Soc. Rev.,* **2007,** 36, 707-718.

[28] G. Decher, J. B. Scheloff, *Multilayer Thin Films: Sequential Assembly of Nanocomposites Materials,* ed. Wiley-VCH Verlag & Co., Weinheim, Germany, **2012.**

[29] G. Decher and J. Schmitt, *Prog. Colloid Polym. Sci.,* **1992**, 89, 160-164.

[30] D. Ingersoll, P. J. Kulesza, L. R. Faulkner, *J. Electrochem. Soc.,* **1994**, 141, 140-147.

[31] S. Liu, D. Volkmer, D. G. Kurth, *J. Cluster Sci.,* **2003**, 14, 405-419.

[32] N. A. Kotov, I. Dekany, J. H. Fendler, *J. Phys. Chem.,* **1995**, 13, 13065-13069.

[33] M. M. Ling, K. Y. Wang, T. S. Chung, *Ind. Eng. Chem. Res.,* **2010,** 49, 5869-5876.

[34] A. A. Mamedov, N. A. Kotov, M. Prato, D. M. Guldi, J. P. Wicksted, A. Hirsch, *Nat. Mater.,* **2002**, 1, 190-194.

[35] C. Jiang, H. Ko, V. V. Tsukruk, *Adv. Mater.,* **2005**, 17, 2127-2131.

[36] S. W. Keller, H. N. Kim, T. E. Mallouk, *J. Am. Chem. Soc.,* **1994**, 116, 8817.

[37] E. R. Kleinfeld, G. S. Ferguson, *Science*, **1994**, 265-370.

[38] T. M. Cooper, A. L. Campell, R. L. Crane, *Langmuir*, **1995**, 11, 2713-2718.

[39] T. A. He, R. Valluzi, K. Yang, T. Dolukhanyan, C. Sung, J. Kumar, S. K. Tripathy, L. Samuelson, L. Balogh, D. A. Tomalia, *Chem. Mater.,* **1999**, 11, 3268.

[40] K. Araki, M. J. Wagner, M. S. Wrighton, *Macromolecules*, **1996**, 16, 5392-5397.

[41] Y. Lvov, G. Decher, G. Sukhorukov, *Macromolecules*, **1993**, 26, 5396.

[42] J. D. Hong, K. Lowack, J. Schmitt, G. Decher, *Prog. Colloid Polym. Sci.,* **1993**, 93, 98.

[43] Y. Lvov, K. Ariga, T. Kuhitake, *Chem. Lett.,* **1994,** 23, 23.

[44] Y. Lvov, K. Ariga, I. Ichinose, T. Kunitake, *J. Am. Chem. Soc.,* **1995**, 117, 6117-6123.

[45] W. Kong, X. Zhang, M. L. Gao, H. Zhou, W. Li, J. C. Shen, *Macromol. Rapid Commun.,* **1994,** 15, 405-409.

[46] P. J. Yoo, K. T. Nam, J. Qi, S. K. Lee, J. Park, A. M. Belcher, P. T. Hammond, *Nat. Mater.*, **2006,** 5, 234.

[47] M. Michel, V. Toniazzo, D. Ruch, Y. Ball, *ISRN Material Science,* **2012.**

[48] W. B. Stockton, M. F. Rubner, *Macromolecules,* **1997,** 30, 2717.

[49] L. Y. Wang, Z. Q. Wang, X. Zhang, J. C. Shen, *Macro. Mol. Rapid Commun.,* **1997,** 18, 509.

[50] S. A. Sukhishvili, S. Granick, *Macromolecules,* **2000,** 122, 9550.

[51] S. A. Sukhishvili, S. Granick, *Macromolecules,* **2002,** 35, 301.

[52] X. Zhang, J. C. Shen, *Adv. Matter.,* **2006,** 18, 1672.

[53] M. L. Gao, X. X. Kong, X. Zhang, J. C. Shen, *Chem. J. Cin. Univ.,* **1993,** 14, 1182.

[54] G. Decher, *Science,* **1997,** 277, 1232.

[55] W. Kong, X. Zhang, M. L. Gao, H. Zhou, W. Li, J. C. Shen, *Macromol. Rapid Commun.,* **1994,** 15, 405.

[56] H. Lee, L. J. Kepley, H. G. Hong, X. Zhang, *J. Am. Chem. Soc.,* **1988,** 110, 618.

[57] P. Kohli, G. J. Blanchard, *Langmuir,* **2000,** 16, 4655.

[58] P. Kohli, K. K. Taylor, J. J. Harris, G. J. Blanchard, *J. Am. Chem. Soc.,* **1998,** 120, 11962.

[59] E. Chan, D. Lee, M. Ng, G. Nu, K. Lee, L. Yu, *J. Am. Soc.,* **2002,** 12438.

[60] I. Ichinose, H. Senzu, T. Kunitake, *Chem. Mater.,* **1997,** 9, 1296.

[61] S. Lee, I. Ichinose, T. Kunitake, *Langmuir,* **1998,** 14, 2857.

[62] G. Acharya, T. Kunitake, *Langmuir,* **2003,** 19, 2260.

[63] Q. Wang, H. Yu, L. Zhong, J. Liu, J. Q. Sun, J. C. Shen, *Chem. Mater.,* **2006,** 18, 1988.

[64] E. H. Kang, P. C. Jin, Y. Q. Yang, J. Q. Sun, J. C. Shen, *Chem. Commun.,* **2006,** 4332.

[65] W. Muler, H. Ringsdorf, E. Rump, G. Wildburg, X. Zhang, L. Angermaier, W. Knoll, M. Liley, J. spinke, *Science,* **1993,** 262, 1706.

[66] J. D. Hong, K. Lowack, J. Scmitt, G. Decher, *Prog. Colloid. Polym. Sci.,* **1993,** 93, 98.

[67] G. Decher, B. Lehr, K. Lowack, J. Schmitt, *Biosens. Bioelectron.,* **1994,** 9, 677.

[68] C. ourdillon, C. Demialle, J. Moiroux, J. M. Saveant, *J. Am. Chem. Soc.,* **1994,** 116, 10328.

[69] Y. Shimazaki, M. Mitsuishi, S. Ito, M. Yamamoto, *Langmuir,* **1997,** 13, 1385.

[70] Y. Shimazaki, M. Mitsuishi, S. Ito, M. Yamamoto, *Langmuir,* **1998,** 14, 1768.

[71] Y. Shimazaki, M. Mitsuishi, S. Ito, M. Yamamoto, *Macromoleculer,* **1999,** 32, 8220.

[72] Y. Shimazaki, S. Ito, *Langmuir,* **2000,** 16, 9478.

[73] L. Cheng, S. J. Dong, *Electrochem. Commun.,* **1999,** 1, 159.

[74] L. Cheng, S. J. Dong, *J. Electroanal. Chem.,* **2000,** 481, 168-176.

[75] D. Zhang, K. Zhang, Y. L. Yao, X. H. Xia, H. Y. Chen, *Langmuir,* **2004,** 20, 7303.

[76] A. Zhuk, S. Pavlukhina, S. A. Sukhishvili, *Langmuir,* **2009,** 25, 24, 14025-14029.

[77] Y. Zhu, J. Shi, W. Shen, X. Dong, J. Fong, M. ruan, Y. Li, *Angew. Chem.,* **2005,** 117, 5213-5217.

[78] Y. Yan, G. K. Such, A. P. R. Johnston, H. Lomas, F. Caruso, *ACS Nano,* **2011,** 5, 4252-4257.

[79] M. Matsusaki, H. Ajiro, T. Kida, T. Serizawa, M. Akashi, *Adv. Mater.,* **2012,** 24, 454-474.

[80] Y. Li, X. Wang, J. Sun, *Chem. Soc. Rev.,* **2012,** 41, 5998-6009.

[81] J. A. Lichter, K. J. Van Vilet, M. F. Rubner, *Macromolecules,* **2009,** 42, 8573-8586.

[82] G. Decher, J. B. Scheloff, *Multilayer Thin Films: Sequential Assembly of Nanocomposites Materials,* ed. Wiley-VCH Verlag & Co., Weinheim, Germany, **2012.**

[83] Y. Lvov, F. Caruso, *Anal. Chem.,* **2001,** 73, 4212-4217.

[84] Y. Lvov, S. Yamada, T. Kunitake, *Thin Solid Films,* **1997,** 300, 107-112.

[85] E. Kang, T. Bu, P. Jin, J. Sun, Y. Yang, J. Shen, *Langmiur,* **2007,** 23, 7594-7601.

[86] G. M. Lowman, H. Tokuhisa, J. L. Lutkenhaus, P.T. Hammond, *Langmiur,* **2004,** 20, 9791-9795.

[87] X. Sheng, L. Zhai, M. F. Rubner, R. E. Cohen, *US Patent 8153233 B2,* **2012,** Massachuetts Institute of Technology, Cambridge, MA (US).

[88] E. Kharlampieva, S. A. Shukhishvili, *Langmuir,* **2003,** 19, 1235.

[89] E. Kharlampieva, S. A. Shukhishvili, *Langmuir,* **2004,** 20, 10712.

[90] S. S. Ono, G. Decher, *Nano. Lett.,* **2006,** 6, 592-598.

[91] G. Ibraz, L. Dohne, E. Donath, H. Moehwald, *Adv. Matter.,* **2001,** 13, 1324.

[92] A. Fery, B. Scholer, T. Cassagneau, F. Caruso, *Langmuir,* **2001,** 12, 3779-3783.

[93] V. Kozzlovskaya, E. Kharlampieva, M. L. Mansfield, S. A. Sukhishvili, *Chem. Mater.,* **2006,** 18, 328-336.

[94] D. Delongchamp, P. Hammond, *Langmuir,* **2004,** 20, 5403-5411.

[95] Z. Zhu, S. A. Sukhishvili, *ACS Nano,* **2009,** 3, 11, 3595-3605.

[96] A. Zhuk, S. Pavlukhina, S. A. Shukhishvili, *Langmuir,* **2009,** 25, 24, 14025-14029.

[97] Z. Zhu, N. Gao, H. Wang, S. A. Sukhishvili, *Journal of Controlled Release,* **2013,** 171, 73-80.

[98] I. Erel-Unal, S. A. Shukhishvili, *Macromolecules,* **2008,** 41, 3962-3970.

[99] E. Kharlampieva, V. Kozlovskaya, J. Tyutina, S. A. Shukhishvili, *Macromolecules,* **2005,** 38, 10523-10531.

[100] W. Wang, L. Liu, X. J. Ju, D. Zerrouki, R. Xie, L. H. Yang, L. Y. Chu, *Chemphschem,* **2009,** 10, 2405-2409.

[101] S. H. Hu, C. H. Tsai, C. F. Liao, D. M. Liu, S. Y. Chen, *Langmuir,* **2008,** 24, 11811-11818.

[102] J. L. Gilmore, X. Li, L. Quan, A. V. Kabanov, *J. Neuroimmune Pharmacol.,***2008,** Jan 22.

[103] T. J. Deerinck, *Toxicol Pathol.,* **2008,** 36, 1, 112-6.

[104] S. J. Son, X. Bai, S. B. Lee, *Drug Discov. Today,* **2007,** 12, 15-16, 650-6.

[105] B.Issa, I. M. Obaidat, B. A. Albiss, Y. Haik, *Int. J. Mol. Sci.,* **2013,** 14, 21266-21305.

[106] A. K. Gupta, M. Gupta, *Biomaterials,* **2005,** 18, 3995-4021.

[107] A. Jordan et al., *Journal of Magnetism and Magnetic Materials,* **2001,** 225, 118-126.

[108] P. Neuberger et al., *Journal of Magnetism and Magnetic Materials,* **2005,** 293, 1, 483-496.

[109] C. Von Zur Muhlen et al., *Atherosclerosis,* **2007,** 193, 1, 102.

[110] Q. A. Pankhurst, K. Connolly, S. K. Jones, J. Dobson, *J. Phys. D,* **2003,** 36, R167-R181.

[111] J. P. Fortin, G. Gaxeau, C. Willhelm, *Eur. Biophys.,* **2008,** 37, 223-228.

[112] R. Hergt, S. Dutz, *J. Magn. Magn. Mater.,* **2007,** 311, 187-192.

[113] S. E. Barry, *Int. J. Hyperth.,* **2008,** 24, 451.

[114] B. Thiesen, A. Jordon, *Int. J. Hyperth.,* **2008,** 24, 467-474.

[115] C. C. Berry, A. S. Curtis, *J. Phys. D,* **2003,** 36, R198-R206.

[116] P. Wust, U. Gneveckow, M. Johannsen, D. Bohner, T. Henkel, F. Kahman, J. Schouli, R. Felix, A. Jordan, *Int. J. Hyperth.,* **2006,** 22, 673-685.

[117] N. A. Spaldin, *Magnetism Materials: Fundamentals and Applications, 2nd Edition, Cambridge University Press.*

[118] M. Ghesian, M. Mozaffari, M. Acet, J. Amighian, *Journal of Magnetism and Magnetic Materials,* **2008,** 320.

[119] R. M. Cornell, U. Schwertfeger, *Wiley VCH,* Weinheim, **2003**.

[120] Pierro A. Dresco, Valdimir S. Zaitser, Richard J. Gambino, Benjamin Chu, *Langmiur,* **1999**, 15, 6.

[121] C. P. Bean, J. D. Livingston, *Journal of Applied Physics,* **1959**, 30, 120-129.

[122] R. R. Baker, J. G. Mather, J. H. Kemnaugh, *Nautre,* **1983**, 301, 79-80.

[123] R. Dronskowski, *Adv. Funct. Mater.*, **2001**, 11, 27.

[124] S. Santra, R. Tapec, N. Theodoropoulou, J. Dobson, S. Hebard, W.Tan, *Langmiur,* **2001**, Vol. 17, No. 10, 2900-2906.

[125] D. Maity, D. C. Agarwal, *Journal of Magnetism and Magnetic Materials,* 308, **2007**, 46-55.

[126] Ming Ming Ling, Kai Yu Wang, Tai Shung Chang, *Ind. Eng. Chem. Res.,* **2010**, 49, 5869-5876

[127] R. Massart, *IEEE Trans. Magn.,* **1981**, 17, 1247.

[128] R. M. Cornell, U. Schwertmann, *Willey-Woch,* ISBN 3-527-29669-7, Weinheim, Germany, **2000**, 55-60.

[129] Jorg Rockenberger, Erik C. Scher, A. Paul Alivisatos, *Journal of American Chemical Society,* **1999**, 121, 11595-111596.

[130] Lee et al, *Journal of Biomedical Materials Research Part: B, Applied Biomaterials,* 79B, **2006**, 142-150.

[131] Beniot P. Pichon, Pierrce Louet, Olivier Felix, Marc Drillon, Sylvie Begin-Colin, Gero Decher, *Chem. Mater.,* **2011**, 23, 3668-3675.

[132] J. Park, K. AN, Y. Hwang, J. G. Park, H. J. Noh, J. Y. Kim, J. H. Park, N. M. Hwang, T. Hyeon, *Nat. Mat.,* **2004**,3, 891-895.

[133] P. Tartaj, M. P. Morales, S. Veintemillas- Verdageur, T. Gonnzalez-Carreno, C. J. Serna, *Handbook of Magnetic Materials,* **2006**, 9, 403.

[134] A. Demotiere, P. Panissod, B. P. Pichon, G. Pourroy, D. Guillon, B. Donnio, S. Begin-Colin, *Nanoscale,* **2011**, 3, 226.

[135] S. F. Chin, S. C. Pang, C. H. Jan, *J. Mater. Environ. Sci.,* **2011**, 3, 299-302.

[136] A. Demortiere, B. Pichon, P. Panissod, B. Donnio, G. Pourroy, D. Gullion, S. Begin-Colin, *Nanaoscale,* **2011**, 255-302.

[137] B. P. Pichon, O. Gerber, C. Lefevre, I, Florea, S. Fleulot, W. Baaziz, M. Pauly, M. Ohlmann, C. Ulhaq, O. Ersen, V. Pierron-Bohnes, P. Panissod, M. Drillon,, S. Begin-Colin, *Chem. Mater.,* **2011,** 23, 2886-2900.

[138] B. P. Pichon, P. Leout, O. Felix, M. Drillon, S. Begin-Colin, G. Decher, *Chem. Mater.,* **2011,** 23, 3668-3675.

[139] Y. Liu, A. Wang, R. O. Claus, *Appl. Phys. Lett.,* **1997,** 71, 16, 2265-2267.

[140] A. Demortiere, S. Buathong, B. P. Pichon, P. Panissod, D. Guillon, S. Begin-Colin, B. Donnio, *Small,* **2010,** 6, 1341.

[141] T. Fried, G. Shemer, G. Markovich, *Adv. Mater.,* **2001,** 13, 1158.

[142] F. Mammeri, Y. L. Bras, T. J. Daou, J. L. Gallani, S. Collins, G. Pourroy, B. Donnio, D. Guillon, S. Begin-Colin, *J. Phys. Chem. B,* **2009,** 113, 734.

[143] M.. Pauly, B. P. Pichon, A. Demortiere, J. Delahaye, C. Leuvrey, G. Pourroy, S. Begin-Colin, *Superlattices Mircostruct.,* **2009,** 46, 195.

[144] M. Pauly, B. P. Pichon, P. A. Albouy, S. Fluetot, C. Leuvrey, M. Trassin, J. L. Gallani, S. Begin-Colin, *J. Mater. Chem.,* **2011,** DOI: 10.1039/cljm12012c.

[145] X. Wang, S. Y. Zhou, Y. Lai, J. Q. Sun, J. C. Shen, *J. Mater. Chem.,* **2010,** 20, 555-560.

[146] F. Shi, S. H. Lui, H. T. Gao, N. Ding, L. J. Dong, W. Tremel, W. Knoll, *Adv. Mater.,* **2009,** 21, 1927-1930.

[147] G. J. Wang, Y. N. Fang, P. Kim, A. Hayek, M. R. Weatherspoon, J. W. Perry, K. H. Sandhage, S. R. Marder, S. C. Jones, *Adv. Func. Mater.,* **2009,** 19, 2768-2776.

[148] L. H. Zhang, Y. M. Zhai, N. Gao, D. Wen, S. Dong, *J. Electrochem. Commun.,* **2008,** 10, 1524-1526.

[149] F. Hua, T. Cui, Y. M. Lvov, *Nano Lett.,* **2004,** 4, 823.

[150] W. Xue, T. Cui, *J. Nanosci. Nanotechnol.,* **2007,** 7, 2647.

[151] L. Yanying, W. Anbo, O. C. Richard, *Appl. Phys. Lett.,* **1997,** 2265-2267.

[152] M. Mazur, A. Barras, V. Kuncser, A. Galatanu, V. Zaitev, K. V. Turchemiuk, P. Woisel, J. Lyskawa, W. Laure, A. Siriwardena, R. Boukherroub, S. Szunerits, *Nanoscale,* **2013,** 5, 2692-2702.

[153] B. P. H. Do, B. D. Nguyen, H. D. Nguyen, P. T. Nguyen, *Adv. Nat. Sci.: Nanosci. Nanotechnology,* **2013,** 4, 045016.

[154] M. Shen, H. Cai, X. Wang, X. Cao, K. li, S. H. Wang, R. Guo, L. Zheng, G. Zhang, X. Shi, *Nanotechnology,* **2012,** 23, 105601.

[155] X. Huang, A. Schmuker, J. Dyke, S. M. Hall, J. Retrum, B. Stein, N. Remmes, D. V. Baxter, B. Gragnea, L. M. Bronstein, *J. Mater. Chem.,* **2009,** 19, 4231-4239.

[156] A. Khan, *Material Letters,* **2008,** 62, 898-902.

[157] S. Mahadevan, G. Gnanaprakash, J. Philip, B. P. C. Rao, T. Jayakumar, *Physica E,* **2007,** 39, 20-25.

[158] H. Qu, D. Caruntu, H. Liu, C. J. O'Connor, *Langmuir,* **2011,** 27, 2271- 2278.

[159] B. Tural, N. Ozkan, M. Volkan, *J. of Phys. And Chem. of solids,* **2009,** 70, 860-866.

[160] M. Mazur, A. Barras, V. kuncser, A. Galatanu, V. Zaitzev, K. V. Turcjeniuk, P. Woisel, J. Lyskawa, W. Laure, A. Siriwardena, R. Boukherroub, S. Szunerits, *Nanoscale,* **2013,** 5, 2692-2702.

[161] M. Baalousha, *Science of the total environment,* **2009,** 407, 2093-2101.

[162] I. Erel-Unal, S. A. Sukhishvili, *Macromolecules,* **2008,** 41, 11, 8737-8744.

 [163] M. G. Albu, M. V. Gluca, M. Gillgrinca, V. Trandafir, L. Popa, C. Cotrut, *Rev. Chim.,* **2009,** 60, Nr. 7, 666-672.

[164] H. Gu, K. Zu, Z. Yang, C. K. Chang, B. Xu, *Chem. Commun.,* **2005,** 4270-4272.

[165] L. Wang, J. Luo, M. M. Maye, Q. Fan, Q. Rendeng, M. H. Engelhard, C. Wang, Y. Lin, C. J. Zhong, *J. Mater. Chem.,* **2005,** 15, 1821-1832.

[166] Y. Maeeda, *Langmiur,* **2001**, 17, 1737.

[167] G. Volgyi, R. Ruiz, K. Box, J. Corner, E. Bosch, K. T. Novak, *Anal. Chim. Acta,* **2007,** 583, 418.

[168] SPARC V3.1, http://ibmlc2.chem.uga.edu/sparc/

[169] J. Barbosa, R. Berges, I. Toro, V. S. Nebot, *Talanta,* **1997,** 44, 1271.

[170]S. Schreiber, M. Savla, D.V. Pelekhov, P. C. Hammel, G. Agarwal, *Small,* **2008,** 4, No. 2, 270-278.

[171] J. Wotshadlo, T. Liebert, J. H. Clement, N. Anspach, S. Hoppener, T. Rudolph, R. Muller, F. H. Schacher, U. S. Schubert, T. Heinze, *Macromol. Biosci.*, **2013,** 13, 93-105.

[172] C. S. Neves, P. Quaresma, P. V. Baptista, P. A. Carvalho, J. P. Araujo, E. Pereira, P. Eaton, *Nanotechnology,* **2010,** 21, 305706.

[173] S. A. Sukhishvili, S. Granick, *Macromolecules,* **2002,** 35, 1, 301-310.

[174] E. Kharlampieva, V. Kozlovskaya, J. Tyutina, S. A. Sukhishvili, *Macromolecules,* **2005,** 38, 25, 10523-10531.

[175] I. Erel, H. E. Karahan, C. Tuncer, V. Butun, A. L. Demirel, *Soft Matter,***2012,** 8, 827-836.